

## 4.0 The Craft of Wavefield Extrapolation

This chapter attends to those details that enable us to do a *high-quality* job of downward continuing wavefields. There will be few new seismic imaging concepts here. There will, however, be interesting examples of pitfalls. And in order to improve the quality of seismic images of the earth, several new and interesting mathematical concepts will be introduced. Toward the end of the chapter a program is prepared to simulate and compare various migration methods.

### The Magic of Color

The first thing we will consider in this chapter is signal strength. Echoes get weaker with time. This affects the images, and requires compensation.

Next, seismic data is colored by filtering. This filtering can be done in space as well as time. Time-series analysis involves the concept of enhancing the signal-to-noise ratio by filtering to suppress some spectral regions and enhance others. Spectral weighting can also be used on wavefields in the space of  $\omega$  and  $k$ . In the absence of noise, wave-equation theory tells us what filters to use. Loosely, the wave equation is a filter with a flat amplitude response in  $(\omega, k)$ -space and a phase response that corresponds to the time delays of propagation. The different regions of  $(\omega, k)$ -space have different amounts of noise. But the different regions need not all be displayed at the strength proposed by the wave equation, any more than data must be displayed with  $\Delta x = \Delta z$ .

An example of the mixture of filter theory and migration theory is provided by the behavior of the spatial Nyquist frequency. Because seismic data is often spatially aliased, this example is not without practical significance. Think of an impulse function with its Nyquist frequency removed. The removal has little relative effect on the impulse, but a massive *relative* effect on the zeroes surrounding the impulse. When migrating an impulse by frequency domain methods, spatial frequencies just below the spatial Nyquist are treated

much differently from frequencies just above it. One is treated as left dip, the other as right dip. This discontinuity in the spatial frequency domain causes a spurious, spread-out response in the space domain shown in figure 1.

The spurious Nyquist noise is readily suppressed, not by excluding the Nyquist frequency from the display, but by a narrow band filter such as used in the display, namely  $(1 + \cos k_x \Delta x)/(1 + .85 \cos k_x \Delta x)$  which goes smoothly to zero at the spatial Nyquist frequency. This filter has a simple triangular representation in the  $x$ -domain.

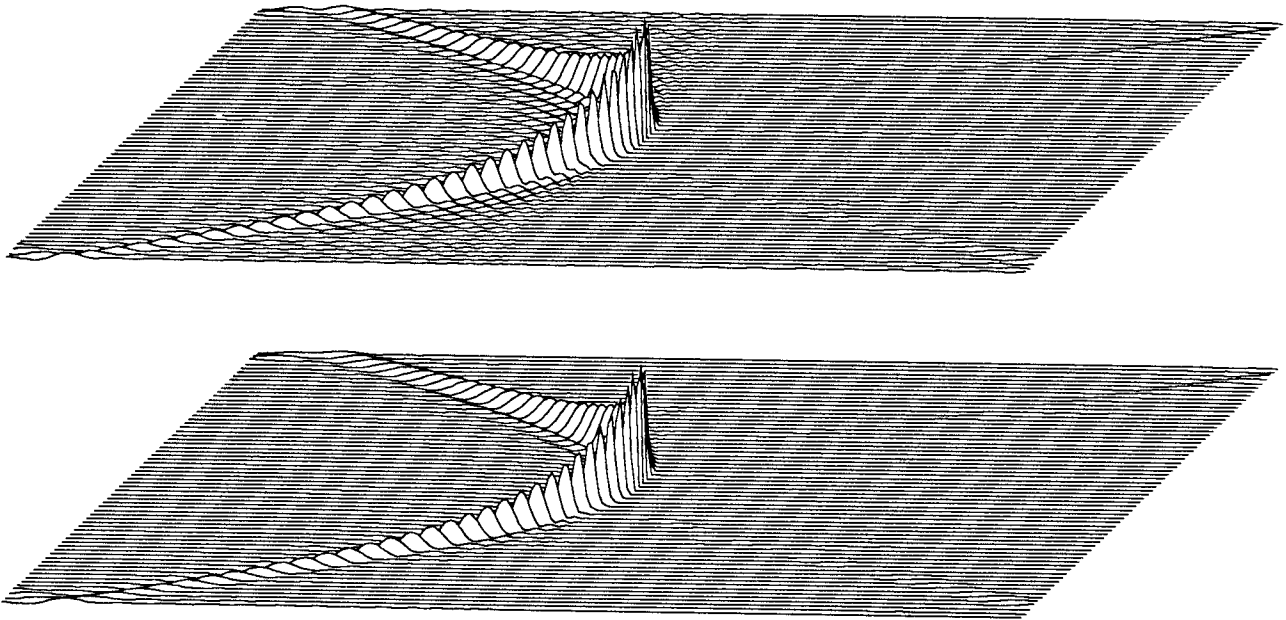


FIG. 4.0-1. Hyperbola amplified to exhibit surrounding Nyquist noise (top) removed by filtering (bottom).

### Survey of Migration Technique Enhancements

In our quest for quality, we will also recall various approximations as we go. Now is the time to see how the use of approximations degrades results, and to discover how to improve those results. Five specific problems will be considered:

- 1 The frequency dispersion that results from the approximation of differential operators by difference operators

- 2 The anisotropy distortion of phase and group velocity that results from square-root approximations
- 3 The effect of truncation at the end of the survey line
- 4 Dips greater than ninety degrees
- 5 Wraparound problems of Fourier transformation
- 6 The effect of  $v(z)$  upon the Stolt method and how to improve the result by stretching

Following study of these approximations, Section 4.6 is a penetrating study of causality, which covers much ground including how Fourier domain migration can simulate the causality intrinsic to time domain migrations. Section 4.7 is the grand summary of techniques. A single program is presented that can simulate diffraction hyperbolas from many different migration methods. This facilitates comparison of techniques and optimization of parameters. Figure 1 and many of the other figures in this chapter were produced with this program, so you should be able to reproduce them.

### A Production Pitfall: Weak Instability from $v(x)$

Some quality problems cannot be understood in the Fourier domain. Unless carefully handled, lateral velocity variation can create instability.

The existence of lateral velocity jumps causes reflections from steep faults. A more serious problem is that the extrapolation equations themselves have not yet been carefully stated. The most accurate derivation of extrapolation equations included in this book so far was done from dispersion relations, which themselves imply velocity constant in  $x$ . The question of how a dispersion relation containing a  $v k_x^2$  term should be represented was never answered. It might be represented by  $v(x, z)\partial_{xx}$ ,  $\partial_x v(x, z)\partial_x$ ,  $\partial_{xx} v(x, z)$  or any combination of these. Each of these expressions, however, implies a different numerical value for the internal reflection coefficient. Worse still, by the time all the axes are discretized, it turns out that one of the most sensible representations leads to reflection coefficients greater than unity and to numerical instability.

A weak instability is worse than a strong one. A strong instability will be noticed immediately, but a weak instability might escape notice and later lead to incorrect geophysical conclusions. Fortunately, a stability analysis leads to a *bulletproof* method in Section 4.8.

## 4.1 Physical and Cosmetic Aspects of Wave Extrapolation

Frequency filtering, dip filtering, and gain control are three processes whose purposes seem to be largely cosmetic: they are used to improve the appearance of data. The criteria used to choose the quantitative parameters of these and similar processes are often vague and relate to human experience or visual perception. In principle, it should be possible to choose the parameters by invoking information theory and using objective criteria such as signal and noise dip spectra. But in routine practice this is not yet being done.

The importance of cosmetic processes is not to be underestimated. On many occasions, for example, a comparison of processing techniques (in order to choose a contractor perhaps?) has been frustrated by an accidental change in cosmetic parameters. These cosmetic processes arise naturally within wave-propagation theory. It seems best to first understand how they arise, and then to build them into the processing, rather than try to append them in some artificial way after the processing. The individual parts of the wave-extrapolation equations will now be examined to show their cosmetic effects.

### t Squared

Echos get weaker with time. To be able to see the data at late times, we generally increase data amplification with time. I have rarely been disappointed by my choice of the function  $t^2$  for the scaling factor. The  $t^2$  scaling function cannot always be expected to work, because it is based on a very simple model. But I find  $t^2$  to be more satisfactory than a popular alternative, the growing exponential. The function  $t^2$  has no parameters whereas the exponential function requires two parameters, one for the time constant, and one for the time at which you must stop the exponential because it gets too large.

The first of the two powers of  $t$  arises because we are transforming three dimensions to one. The seismic waves are spreading out in three dimensions, and the surface area on the expanding spherical wave increases in proportion to the radius squared. Thus the area on which the energy is distributed is increasing in proportion to time squared. But seismic amplitudes are proportional to the square root of the energy. So the basic geometry of energy spreading predicts only a single power of time for the spherical

divergence correction.

An additional power of  $t$  arises from a simple absorption calculation. Absorption requires a model. The model I'll propose is too simple to explain everything about seismic absorption, but it nicely predicts the extra power of  $t$  that experience shows we need. For the model we assume:

- 1 One dimensional propagation
- 2 Constant velocity
- 3 Constant absorption  $Q^{-1}$
- 4 Reflection coefficients random in depth
- 5 No multiple reflections
- 6 White source

These assumptions immediately tell us that a monochromatic wave would decrease exponentially with depth, say, as  $\exp(-\alpha \omega t)$  where  $t$  is travel-time depth and  $\alpha$  is a decay constant which is inversely proportional to the wave quality factor  $Q$ . Many people go astray when they model real seismic data by such a monochromatic wave. A better model is that the seismic source is broad band, for example an impulse function. Because of absorption, high frequencies decay rapidly, eventually leaving only low frequencies, hence a lower signal strength. At propagation time  $t$  the original white (constant) spectrum is replaced by the forementioned function  $\exp(-\alpha \omega t)$  which is a damped exponential function of frequency. The seismic energy available for the creation of an impulsive time function is just proportional to the area under the damped exponential function of frequency. As for the phase, all frequencies will be in phase because the source is assumed impulsive and the velocity is assumed constant. (See Section 4.6 for a causality problem lurking here). Integrating the exponential from zero to infinite frequency provides us with an inverse power of  $t$  thus completing the justification of a  $t^2$  divergence correction.

It is curious that the shape of the expected seismogram envelope  $t^{-2}$  does not depend on the dissipation constant  $\alpha$ . But changing the spectrum of the seismic source does change the shape of the envelope. It is left for an exercise to show that a seismic source with spectrum  $|\omega|^\beta$  implies a divergence correction  $t^{2+\beta}$ .

The seismic velocity increases with depth, so sometimes people who know the velocity may improve the divergence correction by making it a function of velocity (and hence offset) as well as time.

In reality it may be fortuitous that  $t^2$  fits data so well. Actually,  $Q$  generally increases with depth whereas reflection coefficients generally decrease with depth.

### Noise, Surface Waves and Clip

If seismic data contained nothing but reflections, then there would be little trouble plotting it. You would simply multiply by  $t^2$  and then scale so that the largest data values stayed in the available plotting area. In reality there are two problems: 1) noisy traces and 2) noise propagation modes. We have noisy traces because the people in the world won't all be quiet while we listen for echoes. Noise propagation modes are waves trapped in surface layers. So their divergence is in a two-dimensional space rather than the three-dimensional space for reflections. Water noises are additionally strong because of the homogeneity and low absorption of water.

Noises are handled by "clipping" data values at some level lower than the maximum. Clipping means that values larger than the clip value are replaced by the clip value. Since the size of the noise is generally unpredictable, the most reliable method is to use quantiles. Imagine the data points sorted in numerical order by the size of their absolute values. The  $n^{\text{th}}$  quantile is defined as the absolute value that is  $n/100$  of the way between the smallest and largest absolute value. So if data is clipped at the 99<sup>th</sup> percentile, then up to one percent of the data can be infinitely strong noise. I find that most field profiles have less than 10% noisy points. So I often clip at twice the 90<sup>th</sup> percentile. To find the quantile, it is not necessary to fully sort the data. That would be slow. Hoare's algorithm is much faster (see FGDP or Claerbout and Muir [1973] for full reference and more geophysical context).

Different plots have different purposes. It is often important to preserve linearity during processing, but at the last stage — plotting — linearity can be sacrificed to enable us to see all events, large and small. After all, human perceptions are generally logarithmic. In our lab we generally use power laws. I find that replacing data points by their signed square roots generally compresses all signals into a visible range. When plotting field profiles with a very close trace spacing, it may be better to use the signed cube roots. More generally, we do non-linear gain with

$$\text{Display} = \text{sgn}(\text{Data}) | \text{Data} |^\gamma \quad (1)$$

Gamma is a term in photography to describe nonlinearity of photographic film. Most of the data plots in this book use  $\gamma = 1$ ,  $t^2$  gain, and clip at the 99<sup>th</sup> percentile.

The industry standard approach seems to be AGC (Automatic Gain Control). AGC means to average the data magnitude in some interval and then divide by the magnitude. Although AGC is nonlinear, it is more linear than using  $\gamma$  so it is presumably better if you plan later processing. But with AGC, you lose reversibility and the sense of absolute gain.

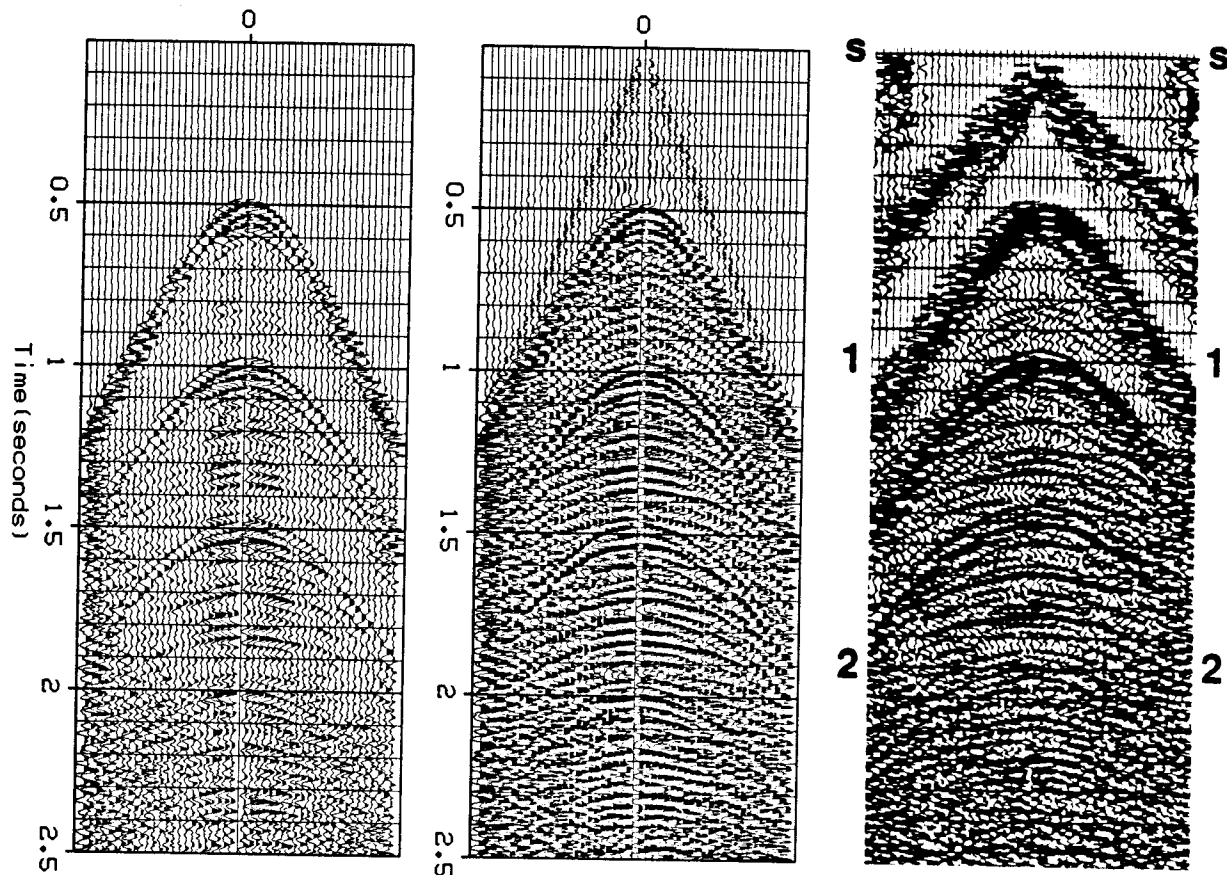


FIG. 4.1-1. Arctic profile from Western Geophysical. Left, with  $t^2$ . Center with  $t^2$  and  $\gamma=0.4$ . Right, with Western's AGC.

Figure 1 is an interesting example. Since it is a split spread, you assume it to be land data. Ships can't push cables in front of them. But the left panel clearly shows marine multiples. The reverberation period is uniform, and there are no reflections before the water bottom. It must be data collected on ice over deep water (375m). From the non-linear gain in the center panel we clearly see a water wave, and before it a fast wave in the ice. There is also weak low-velocity, low-frequency "ground roll" on the ice. There are also some good reflections.

### Complex Velocity in the 5° Equation

The 5° equation, namely,

$$\frac{\partial P}{\partial z} = \frac{1}{v} \frac{\partial P}{\partial t} \quad (2a)$$

$$i k_z = \frac{-i\omega}{v} \quad (2b)$$

states that a wavefront will take some time to get from one depth to another. With velocity  $v$  being a real constant, waves controlled by (2) propagate without change in form. In practice waveform changes are observed. So  $v$  should not be a real constant. An imaginary part of the velocity would cause attenuation. A frequency-dependent velocity would cause frequency dispersion.

### Absorption

A basic model arises when  $v(\omega)$  is defined by the equation

$$\frac{-i\omega}{v(\omega)} = \frac{\omega_0}{v_0} \left( \frac{-i\omega}{\omega_0} \right)^{1-\epsilon} \quad (3)$$

For  $\epsilon = 0$ , equation (3) gives a constant velocity. Equation (3) models the so-called causal, constant  $Q$  attenuation where  $Q^{-1} = \tan \pi\epsilon$  (see Section 4.6). Figure 2 shows an example of a synthetic seismogram generated by the exploding-reflector model using equations (2) and (3).

Equation (3) creates attenuation by introducing an imaginary part into the velocity. The main effect of this attenuation is to weaken the arrivals at late time. A secondary effect is to make the frequency content of late arrivals lower. A tertiary effect is this: It happens that the requirement of causality forces the real part of the velocity to be slightly frequency-dependent. In the figure, this slight frequency-dependence is evidenced by the "rise time" on each pulse being faster than the "fall time." This means that the high frequencies are traveling slightly faster than the low frequencies. In practice, this tertiary effect is rarely noticeable.

In making earth images, earth dissipation might be compensated by amplifying high-frequency energy during downward continuation. This might be done just like migration, except that  $k_z = -\sqrt{\omega^2/v^2 - k_x^2}$  would be replaced by something like  $ik_z = (-i\omega)^{1-\epsilon}$ . In practice, however, no one would really do this, since it would amplify high frequency noise. This raises the issue of signal-to-noise ratio.

Noise isn't simply an ambient random fluctuation. It is mainly repeatable if the data is reshot. Noise is anything for which we have no satisfactory model. On a practical level, time-variable filters are often used to select pleasing time-variable passbands. Equations (2) and (3) could be used for this implementation of time-variable filters, but it would be an oversimplification



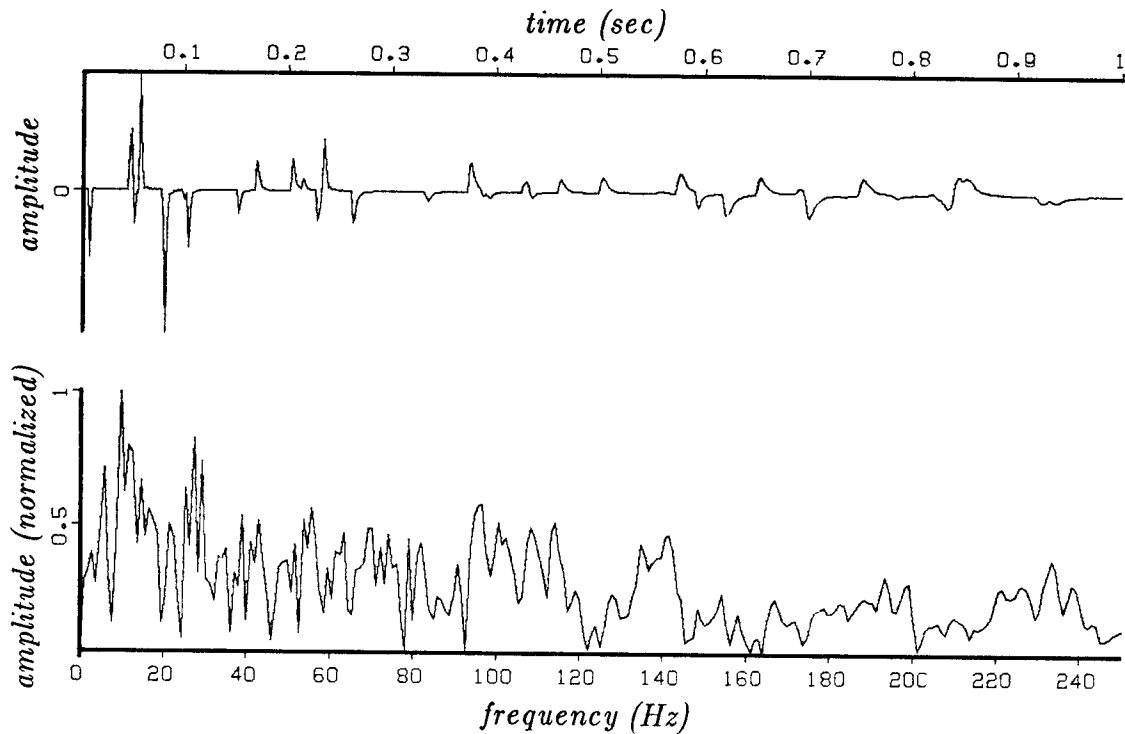


FIG. 4.1-2. Synthetic seismogram for an earth with  $Q \approx 100$ . (Hale)

to view their use as compensation for the earth  $Q$ .

### Dispersion

The frequency-dependence of velocity in the case of surface waves is more dramatic. For example, a frequency-dependent velocity is given by the equation

$$\frac{-i\omega}{v(\omega)} = \frac{-i\omega}{v_0} \sqrt{1 + \omega_0^2/\omega^2} \quad (4)$$

Figure 3a contains some frequency-dispersive ground roll. In figure 3b the dispersion has been backed out by a migration-like process. One difference between this process and migration is that migration extrapolates down the  $z$ -axis whereas in figure 3b the extrapolation is along the  $x$ -axis. (The extrapolation direction is really just in the computer). Each trace in figure 3b is processed separately. In migration, data  $p(t, z=0)$  is extrapolated to an image  $p(t=0, z)$  using a dispersion relation  $k_z = -\sqrt{\omega^2/v^2 - k_x^2}$ . In this process, data  $p(t, x=0)$  is extrapolated to an image  $p(t=0, x)$  using a dispersion relation like  $k_x = f(\omega/v)$ . After this

pseudomigration a pseudodiffraction is done with a *constant* velocity. The total effect is to undo the frequency dispersion. Finally, it is possible to see that the noise consists of two separate events. Techniques resembling this one were first used to locate faults in coal seams (Beresford-Smith and Mason [1980]).

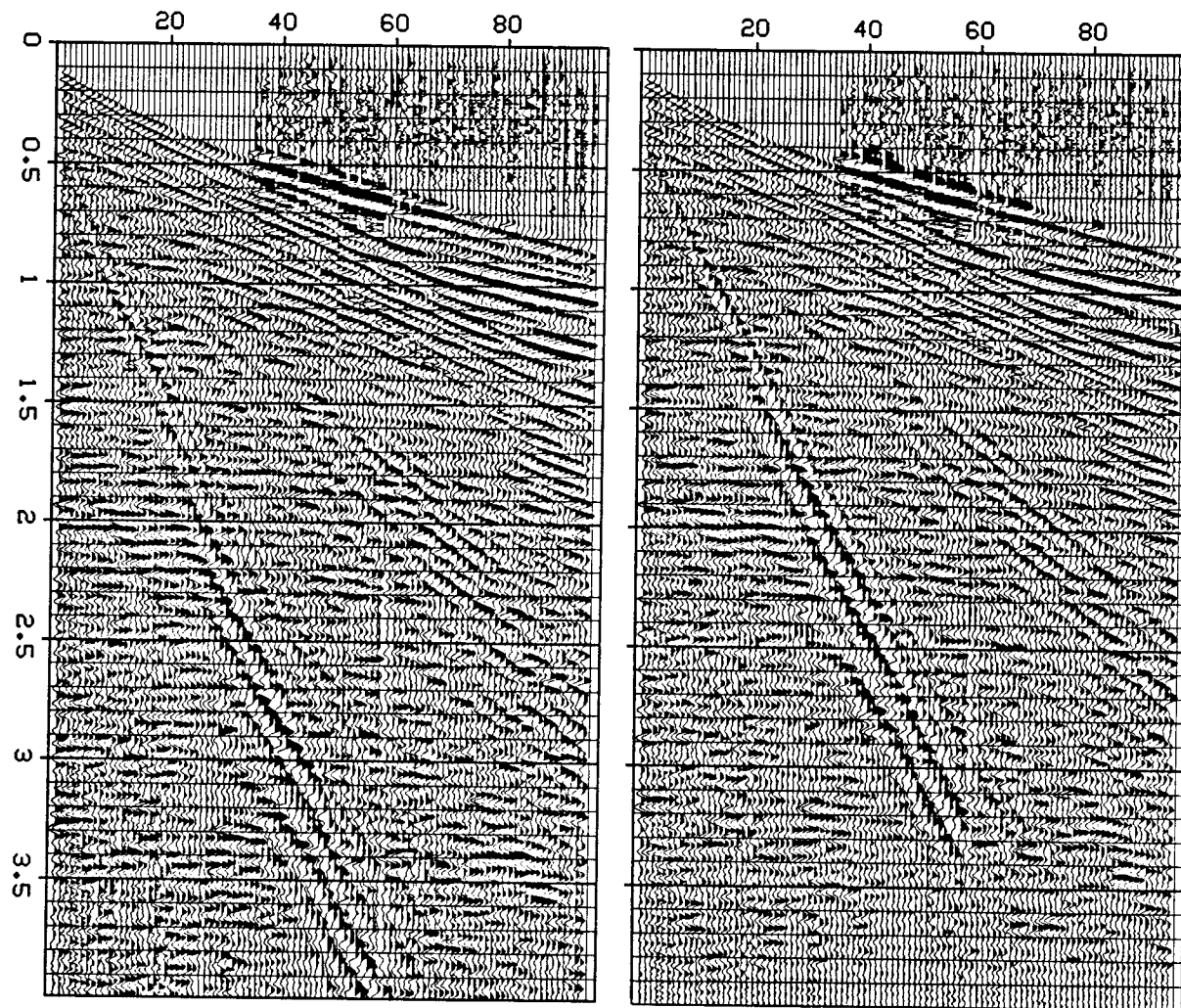


FIG. 4.1-3. Dispersive surface wave (left), with the frequency dispersion backed out (right). Bottom shows two arrivals, the direct, straight-line arrival, and a hyperbola flank. The hyperbola represents sidescatter that must come from some object on the earth's surface off to the side of the survey line. (Conoco, Sword)

### False Semicircles in Migrated Data

Dip filtering can be used to suppress multiples. Section 5.5 will show that multiples are unlike primaries in one important respect: their strength may change rapidly in the horizontal direction. They need not be spread out into broad diffraction hyperbolas as primaries must. This difference arises because multiples often spend much time focusing themselves in the irregular, near-surface areas. Common evidence for this behavior is contained in the appearance of wide-angle migrated sections. Such sections often show semicircular arcs coming all the way up to the surface. These arcs warn that something is wrong. The arcs could result from multiples, statics, or unexplained impulsive noise. In any case, they could be partially suppressed without touching primaries.

### Zapping Multiples in Dip Space

Think of the migration of a common-depth-point stack as downward continuation in  $(\omega, k_x, z)$ -space. Ordinarily, velocity increases with depth. As the downward continuation proceeds, the velocity cutoff along the evanescent line bites out more and more area from the  $(\omega, k_x)$ -space (Section 1.4). Energy beyond this cutoff does not fit the primary wave-propagation model, and it should be suppressed as soon as it is encountered. Such noise suppression can lead to a large drop in total power at late times.

### Mixed Appearance of Dip-Filtered Data

An objection often raised against dip filtering is that it can give data a *mixed* appearance. *Mixed* means that adjacent channels appear to have been averaged and that they are no longer independent. This is indeed an effect of dip filtering, and it is inevitable at late times since the horizontal resolving power of reflection data decreases with time. There are two reasons for decreasing lateral resolution. First, dissipation causes high frequencies to disappear. Second, ray bending causes the angular aperture to decrease for deeper sources. (Section 1.2 and Section 1.5). It is unrealistic to ignore this fundamental limitation and imagine that adjacent channels should have an appearance of independence. If a mixed appearance is to be avoided for display purposes, then I advocate removing the low-velocity, coherent, signal-generated noise and replacing it by low-velocity, incoherent, Gaussian, random noise. Many plotters lose dynamic range at close trace spacing, and random noise can tend to restore it.

### Accentuating Faults

It often happens that the location of oil is controlled by faulting. But the dominating effect of stratified reflectors may overwhelm the weak diffraction evidence of faulting. A cosmetic process could weaken the zero and small dips, accentuating dips in the range of  $10^\circ$  to  $60^\circ$ , and then suppress the wide angles and evanescent energy. As with frequency filtering, sharp cutoffs are not desirable because of the implied long (and in space, wide) impulse response.

### Dip Filtering

Dip filtering is conveniently incorporated into the wave extrapolation equations. Instead of initializing the Muir expansion with  $ik_z = -i\omega r_0$  we use  $ik_z = \epsilon - i\omega r_0$ . (Recall Section 2.1 that  $r_0$  is the cosine of an exactly fitting angle). For the  $15^\circ$  equation we have

$$i k_z^{(15)} v = -i \omega + \frac{v^2 k_x^2}{\epsilon - i \omega (r_0 + 1)} \quad (5a)$$

For the  $45^\circ$  equation we have

$$i k_z^{(45)} v = -i \omega + \frac{v^2 k_x^2}{-i \omega 2 + \frac{v^2 k_x^2}{\epsilon - i \omega (r_0 + 1)}} \quad (5b)$$

Figures 4 and 5 show hyperbolas of diffraction for the  $15^\circ$  and  $45^\circ$  equations with and without the dip filtering parameter  $\epsilon$ .

### Gain Control Does Dip Filtering Too

Echoes arriving late are weaker than echoes arriving early. Thus data is ordinarily scaled for plotting using some time-variable scale. Should migration be done before or after this scaling? The results will differ in an interesting way. The top part of the hyperbola has flat dip, whereas the asymptotes, which come later, have steep dip. So, amplification of late information coincidentally amplifies the steep dips. I think the main effect of choosing to do migration before or after scaling is selection of the dip spectrum in the final display. A pedantically correct approach is to migrate first and scale second, but the result will be weaker in dip and fault information than the answer obtained by scaling first and migrating second. A side benefit of the latter method is that you can save computer memory by storing scaled values as

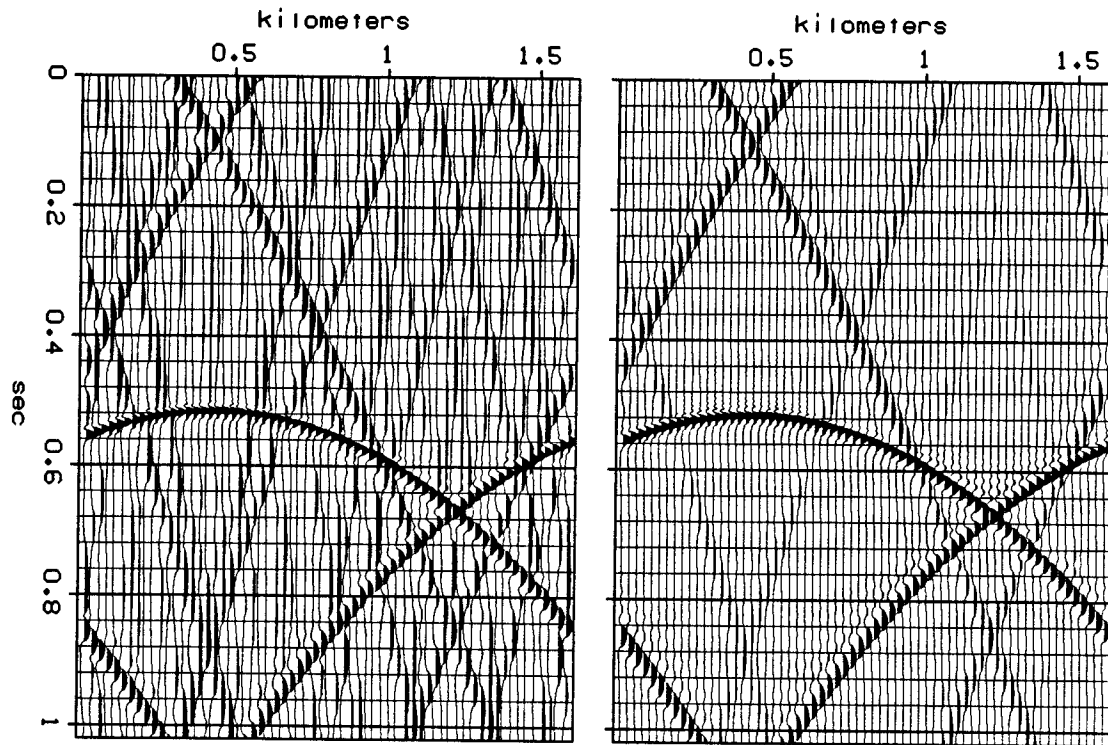


FIG. 4.1-4. Diffraction hyperbolas of the  $15^\circ$  equation without dip filtering (left), and with dip filtering (right).

short integers. I used 16 bit integer storage in my pioneering work. Computations and local storage used 32 bit floating point arithmetic. I see little justification for 32 bit storage generally used today. We can't interpolate between channels to 4 bits of accuracy.

### Rejection by Incoherence or Rejection by Filtering?

It is a pitfall to judge a supposed noncosmetic process by a cosmetic effect. I once got caught. The process was migration before stack. The feature that was deemed desirable was the relative strength of the steepest clear event on the record, a fault-plane reflection. But even gain control can affect dip spectra! I hoped the process was working by correctly eliminating some of the rejection of steep dips by CDP stack. Perhaps it was, but how could I know whether this was happening or whether dips were being accidentally enhanced by spatial filtering?

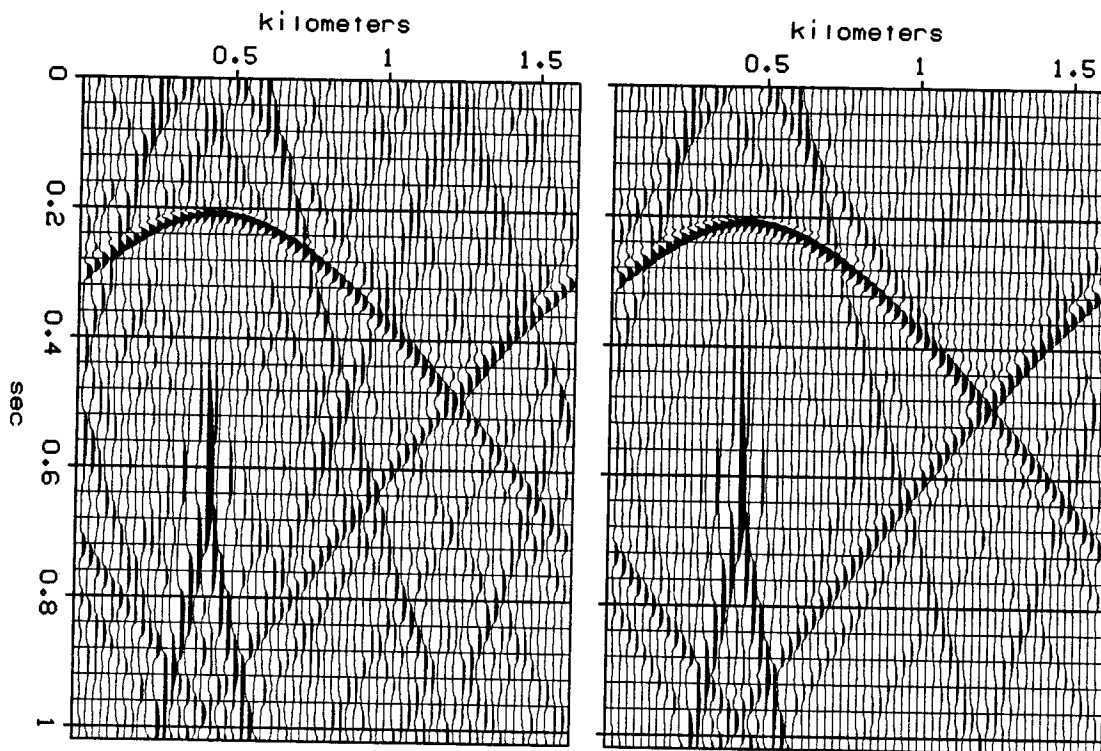


FIG. 4.1-5. Diffraction hyperbolas of the  $45^\circ$  equation without dip filtering (left), and with dip filtering (right).

### Spatial Scaling before Migration

Scaling on the time axis before migration can be advantageous. What about scaling on the space axis? The traditional methods of scaling that are called *automatic gain control* (AGC) deduce a scaling divisor by smoothing the data envelope (or its square or its absolute value) over some window. Such scaling can vary rapidly from trace to trace, so concern is justified that diffractions might be caused by lateral jumps in the scaling function. On the other hand, there might be good reasons for the scale to jump rapidly from trace to trace. The shots and geophones used to collect land data normally have variable strength and coupling, and these problems affect the entire trace.

A model must be found that respects both physics and statistics. I suggest allowing for gain that is slowly time-variable and shots and geophones of arbitrarily variable strength, but I also prefer to regard an impulse as evidence that the earth really can focus. For example, data processing with this model can be implemented by smoothing the scaling *envelope* with the filter

$$1 - \frac{\omega^2}{\alpha + \omega^2} \frac{k_x^2}{\beta + k_x^2} \quad (6)$$

Filter cutoff parameters are  $\alpha$  and  $\beta$ . When the scaling envelope has been smoothed with this filter, it no longer varies rapidly with both  $x$  and  $t$ , although it can vary with either one or the other. This filter (6) can be economically implemented using the tridiagonal algorithm.

### Exponential Scaling

Exponential scaling functions have some ideal mathematical properties. (If you are not familiar with  $Z$ -transforms, you should read Section 4.6 or FGDP before proceeding.) Take the  $Z$ -transform of a time function  $a_t$ :

$$A(Z) = a_0 + a_1 Z + a_2 Z^2 + \dots \quad (7)$$

The exponentially gained time function is defined by

$$\uparrow A(Z) = a_0 + a_1 e^\alpha Z + a_2 e^{2\alpha} Z^2 + \dots \quad (8)$$

The symbol  $\uparrow$  denotes exponential gain. Mathematically,  $\uparrow$  means that  $Z$  is replaced by  $e^\alpha Z$ . Polynomial multiplication amounts to convolution of the coefficients:

$$C(Z) = A(Z)B(Z) \quad (9)$$

By direct substitution,

$$\uparrow C = (\uparrow A)(\uparrow B) \quad (10)$$

This means that exponential gain can be done either before or after convolution. You may recall from Fourier transform theory that multiplication of a time function by a decaying exponential  $\exp(-\alpha t)$  is the equivalent of replacing  $-i\omega$  by  $-i\omega + \alpha$  in the transform domain.

Specialize the downward-continuation operator  $\exp(ik_z z)$  to some fixed  $z$  and some fixed  $k_x$ . The operator has become a function of  $\omega$  that may be expressed in the time domain as a filter  $a_t$ . Hyperbola flanks move *upward* on migration. So the filter is *anticausal*. This is denoted by

$$A(Z) = a_0 + a_{-1} \frac{1}{Z} + a_{-2} \frac{1}{Z^2} + \dots \quad (11)$$

The large negative powers of  $Z$  are associated with the hyperbola flanks. Exponentially boosting the coefficients of positive powers of  $Z$  is associated with diminishing negative powers — so  $\uparrow A$  is  $A$  with a weakened tail — and tends to attenuate flanks rather than move them. Thus  $\uparrow A$  may be described as viscous.

From a purely physical point of view cosmetic functions like gain control and dip filtering should be done after processing, say,  $\uparrow(AB)$ . But  $\uparrow(AB)$  is equivalent to  $(\uparrow A)(\uparrow B)$ , and the latter operation amounts to using a viscous operator on exponentially gained data. In practice, it is common to forget the viscosity and create  $A(\uparrow B)$ . Perhaps this means that dipping events carry more information than flat ones.

### The Substitution Operator

The  $\uparrow$  operator has been defined as the substitution  $Z \rightarrow Z e^\alpha$ . The main property of this operator is that if  $C = A B$ , then  $\uparrow C = (\uparrow A)(\uparrow B)$ . This property would be shared by any algebraic substitution for  $Z$ , not just the one for exponential gain. Another simple substitution can be used to achieve time-axis stretching or compression. For example, replacing  $Z$  by  $Z^2$  stretches the time axis by two. Yet another substitution, which has a deeper meaning than either of the previous two, is the substitution of the constant  $Q$  dissipation operator  $(-i\omega)^\gamma$ . In summary:

Substitutions for $Z$ -Transform Variable $Z$ [ all preserve $C(Z) = A(Z)B(Z)$ ]	
Exponential growth	$Z \rightarrow Z e^\alpha$ $(i\omega \rightarrow i\omega + \alpha)$
Time expansion ( $\alpha > 1$ )	$Z \rightarrow Z^\alpha$
(Inverse) Constant $Q$ dissipation	$-i\omega \rightarrow (-i\omega)^\gamma$

### EXERCISES

1. Use a table of integrals to show that a seismic source with spectrum  $|\omega|^\beta$  implies a divergence correction  $t^{2+\beta}$ .
2. Assuming that  $t^2$  is a suitable divergence correction for field profiles, what divergence correction should be applied to CDP stacks?
3. How is the  $t^2$  correction altered for water of travel time depth  $t_0$ ? Assume the  $Q$  of water is infinite.
4. Consider a source spectrum  $e^{-\beta|\omega|}$ . How is the  $t^2$  correction altered?



5. The spectrum in figure 2 shows high frequencies smoother than low frequencies. Explain.
6. State some criteria that can be used in the selection of the cutoff parameters  $\alpha$  and  $\beta$  for the filter (6).

## 4.2 Anisotropy Dispersion and Wave-Migration Accuracy

Two distinct types of errors are made in wave migration. Of greater practical importance is *frequency dispersion*, which occurs when different frequencies propagate at different speeds. This may be reduced by improving the accuracy of finite-difference approximations to differentials. Its cure is refinement of the differencing mesh. See Section 4.3.

Of secondary importance, and the subject of this section, is *anisotropy dispersion*. Anisotropic wave propagation is waves going different directions with different speeds. In principle, anisotropic dispersion is remedied by the Muir square-root expansion. In practice, the expansion is generally truncated at either the 15° or 45° term, creating anisotropy error in data processing. The reasons often given for truncating the series and causing the error are (1) the cost of processing and (2) the larger size of other errors in the overall data collection and processing activity. Anisotropy error should be studied in order to (1) recognize the problem when it occurs and (2) understand the basic trade-off between cost and accuracy.

Anisotropy is often associated with the propagation of light in crystals. In reflection seismology, anisotropy is occasionally invoked to explain small discrepancies between borehole velocity measurements (vertical propagation) and velocity determined by normal moveout (horizontal propagation). These fundamental, physical anisotropies and the subject of this section, anisotropy in data processing, share a common mathematical and conceptual basis.

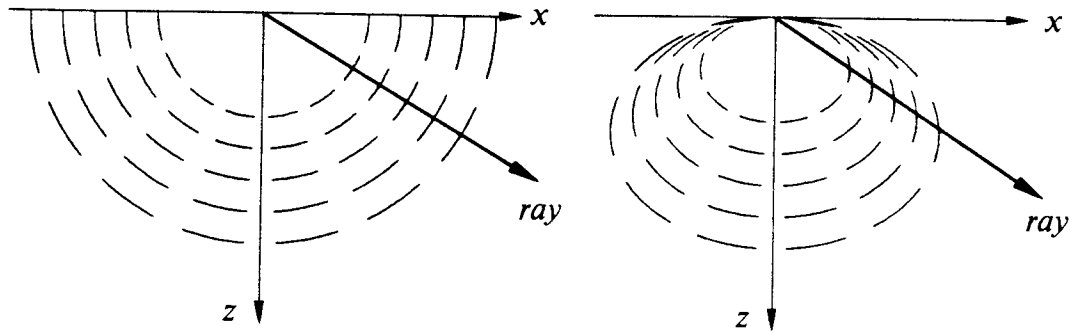


FIG. 4.2-1. Wavefronts in an isotropic medium (left) and an anisotropic medium (right). Note that on the right, the rays are not perpendicular to the wavefronts. (Rothman)

### Rays not Perpendicular to Fronts

Anisotropy means that waves propagating in different directions propagate at different speeds. Anisotropy does *not* mean that velocity is a function of spatial location, and thus anisotropy does not cause rays to bend. The peculiar thing about anisotropy is that rays are not perpendicular to wavefronts. Figure 1 illustrates this idea. The diagram on the left shows spherical wavefronts emanating from a point source at the origin. This is the usual, isotropic case. The diagram on the right shows the nonspherical wavefronts of the  $15^\circ$  migration equation. Note that near the  $z$ -axis they are nearly spherical, but further away they do a poor job of matching a sphere with its center at the origin.

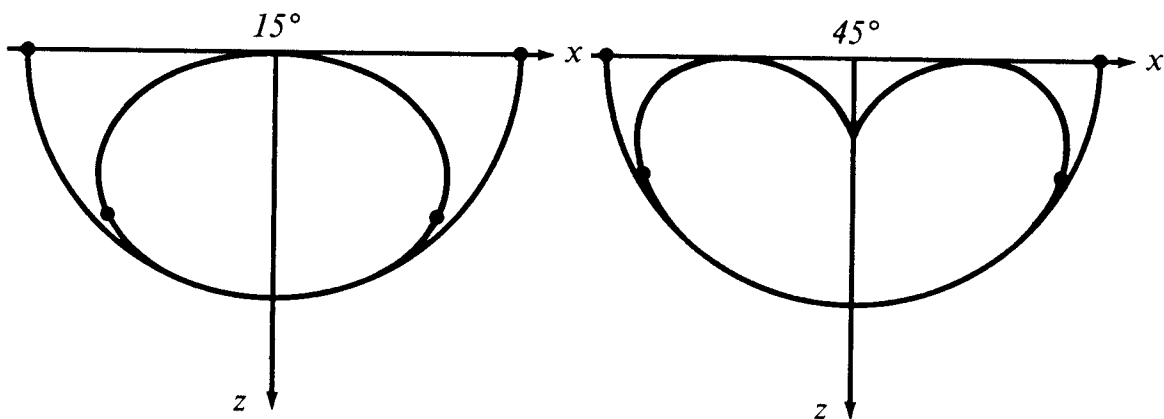
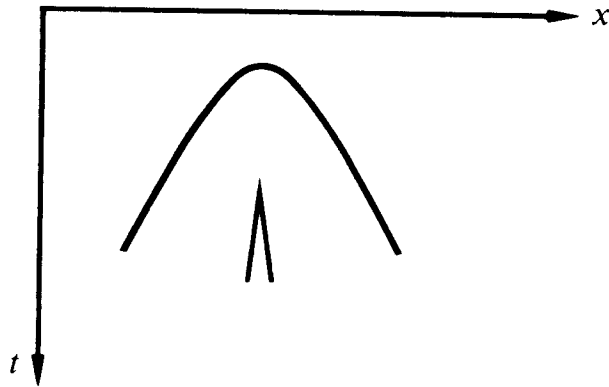


FIG. 4.2-2. Wavefronts of  $15^\circ$  (left) and  $45^\circ$  (right) extrapolation equations, inscribed within the exact semicircle. Waves with  $\sin \theta = vk_x/\omega = \pm 1$  are marked with small dots. Evanescent energy lies beyond the dots. (Rothman)

The ideal wavefront from a Huygens secondary source is a semicircle. The secondary source that results from the  $15^\circ$  extrapolation equation is an ellipse. The secondary source that results from the  $45^\circ$  extrapolation equation is an interesting, heartlike shape. These are drawn in figure 2. In practice, the top parts of the ellipse and the heart are rarely observed because they are in the evanescent zone, and the  $x$ -axis is seldom refined enough for them to be below the aliasing frequency. The center of the heart is sometimes seen in the  $(x, t)$ -plane when the  $45^\circ$  program is used. It is shown by a line drawing in figure 3 and shown using a  $45^\circ$  diffraction program in figure 4.

FIG. 4.2-3.  $45^\circ$  heart theory. The cusp arises in the evanescent region. (Rothman)



### Wavefront Direction and Energy Velocity

In ordinary wave propagation, energy propagates perpendicular to the wavefront. When there is anisotropy dispersion, the angle won't be perpendicular.

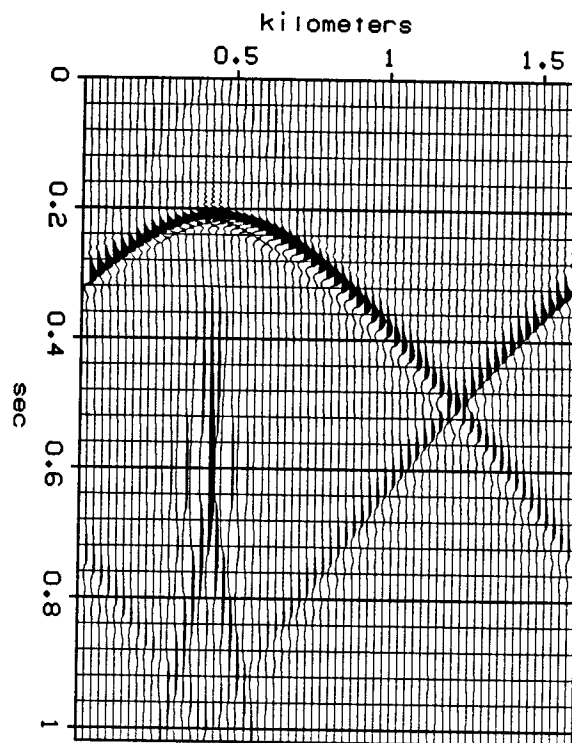
The apparent horizontal velocity seen along the earth's surface is  $dx/dt$ . The apparent velocity along a vertical, e.g., as seen in a borehole, is  $dz/dt$ . By geometry, both of these apparent speeds exceed the wave speed. The vector perpendicular to the wavefront with a magnitude inverse to the velocity is called the slowness vector:

$$\text{slowness vector} = \left( \frac{dt}{dx}, \frac{dt}{dz} \right)$$

The phase velocity vector is defined to go in the direction of the slowness vector, but have the speed of the wavefront normal. More precisely, the phase velocity vector is the slowness vector divided by its squared magnitude:

$$\text{phase velocity} = \frac{\left( \frac{dt}{dx}, \frac{dt}{dz} \right)}{\left[ \left( \frac{dt}{dx} \right)^2 + \left( \frac{dt}{dz} \right)^2 \right]^{1/2}}$$

FIG. 4.2-4. Impulse response of the  $45^\circ$  wave-extrapolation equation. The arrival before  $t_0$  is a wraparound.



For a disturbance of sinusoidal form, namely,  $\exp(i\phi) = \exp(-i\omega t + ik_x x + ik_z z)$ , the phase  $\phi$  may be set equal to a constant:

$$0 = d\phi = -\omega dt + k_x dx + k_z dz$$

Thus, in Fourier space the slowness vector is

$$\text{slowness vector} = \left( \frac{k_x}{\omega}, \frac{k_z}{\omega} \right) \quad (1a)$$

The direction of energy propagation is somewhat more difficult to derive, but it comes from the so-called group velocity vector:

$$\text{group velocity} = \left( \frac{\partial}{\partial k_x}, \frac{\partial}{\partial k_z} \right) \omega(k_x, k_z) \quad (1b)$$

For the scalar wave equation  $\omega^2/v^2 = k_x^2 + k_z^2$ , the group velocity vector and the phase velocity vector turn out to be the same, as can be verified by differentiation and substitution. The most familiar type of dispersion is frequency dispersion, i.e. different frequencies travel at different speeds. Later in this section it will be shown that the familiar ( $15^\circ$ ,  $45^\circ$ , etc.) extrapolation equations do not exhibit frequency dispersion. That is, as functions of  $\omega$  and angle  $k_x/\omega$ , the velocities in these equations do not depend on  $\omega$ . In other words, the elliptical and heart shapes in figure 2 are not frequency-dependent.

An interesting aspect of anisotropy dispersion is that energy appears to be going in one direction when it is really going in another. An exaggerated instance of this occurs when the group velocity has a downward component and the phase velocity has an upward component. Figure 5, depicting the dispersion relation of the  $45^\circ$  extrapolation equation, shows an example. A slowness vector, which is in the direction of the wavefront normal, has been selected by drawing an arrow from the origin to the dispersion curve. The corresponding direction of group velocity may now be determined graphically by noting that group velocity is defined by the gradient operator in equation (1b). Think of  $\omega$  as the height of a hill from which  $k_z$  points south and  $k_x$  points east. Then the dispersion relation is a contour of constant altitude. Different numerical values of frequency result from drawing figure 5 to different scales. The group velocity, in the direction of the gradient, is perpendicular to the contours of constant  $\omega$ .

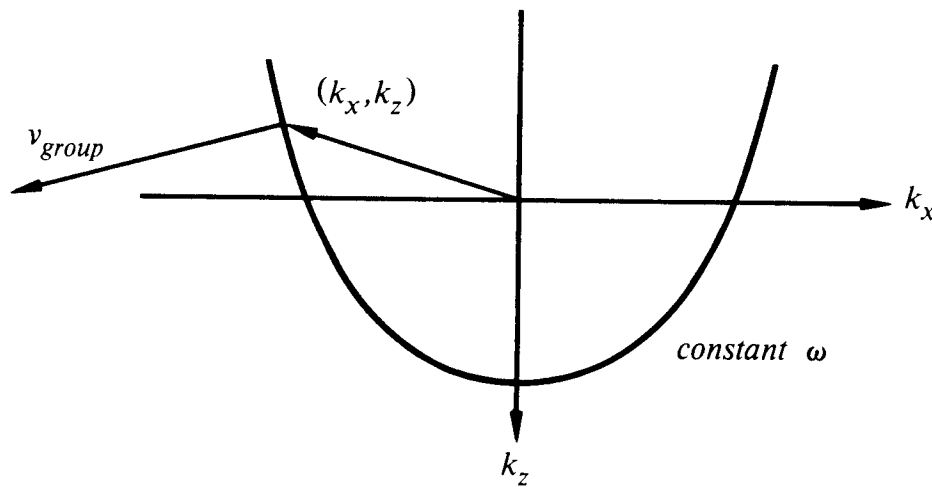


FIG. 4.2-5. Dispersion relation for downgoing extrapolation equation showing group velocity vector and slowness vector. (Rothman)

The anisotropy-dispersion phenomenon can be most clearly recognized in a movie, although it can be understood on a single frame, as in figure 6. The line drawing interprets energy flow from the top, through the prism, reflecting at the  $45^\circ$  angle, reflecting from the side of the frame, and finally entering an area of the figure that is sufficiently large and uncluttered for the phase fronts to be recognizable as energy apparently propagating upward but really propagating downward.

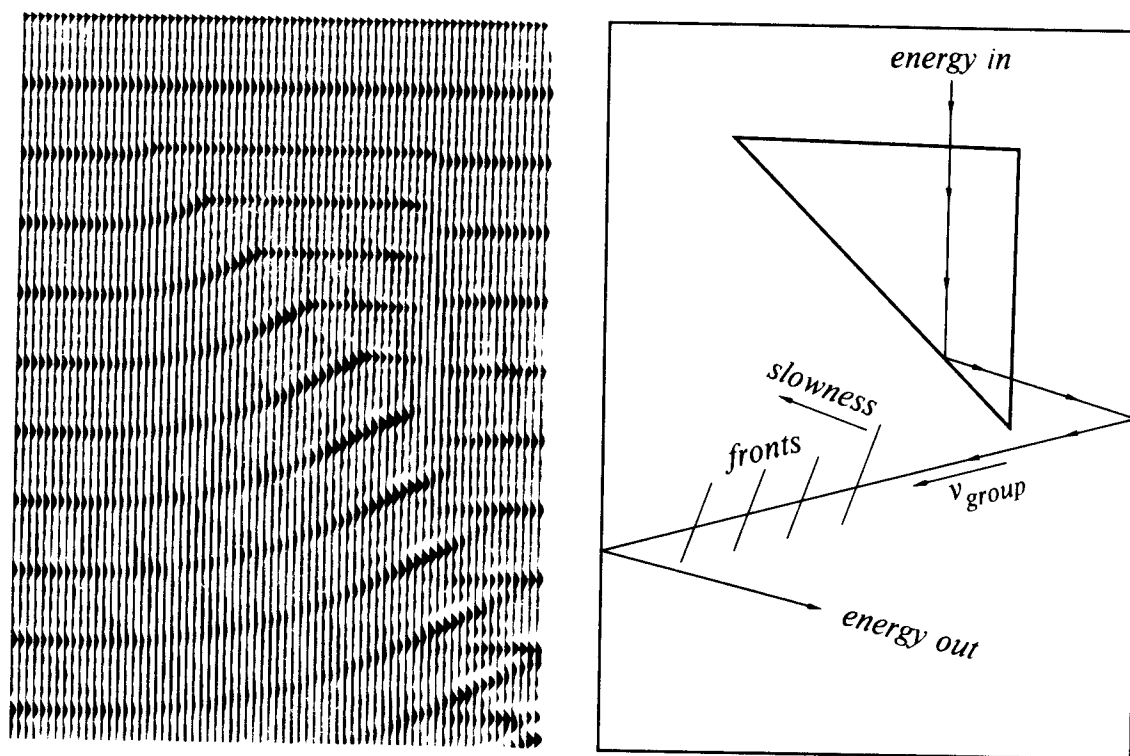


FIG. 4.2-6. Plane waves of four different frequencies propagating through a right,  $45^\circ$  prism. Left is the wavefield. Right is a ray interpretation that illustrates different directions of energy and wavefront normal. (Estevez)

That neither energy nor information can propagate upward in figure 6 should be obvious when you consider the program that calculates the wavefield. The program does not have the entire frame in memory; it produces one horizontal strip at a time from the strip just above. Thus the movie's phase fronts, which appear to be moving upward, seem curious. Theoretically, wave extrapolation using the  $45^\circ$  equation is not expected to handle angles to  $90^\circ$ . Yet the example in figure 6 shows that these extreme cases are indeed handled, although in a somewhat perverted way.

I once saw a similar circumstance on reflection seismic data from a geologically overthrust area. The data could not be made available to me at the time, and by now is probably long lost in the owner's files, so I can only offer the line drawing in figure 7, which is from memory. The increasing velocity with depth causes the ray to bend upward and reflect from the underside of the overthrust. To see what is happening in the wave equation, it is helpful to draw the dispersion curve at two different velocities, as in figure 8.

Downward continuation of a bit of energy with some particular stepout  $dt/dx = k_x/\omega$  begins at an ordinary angle on the near-surface, slow-velocity

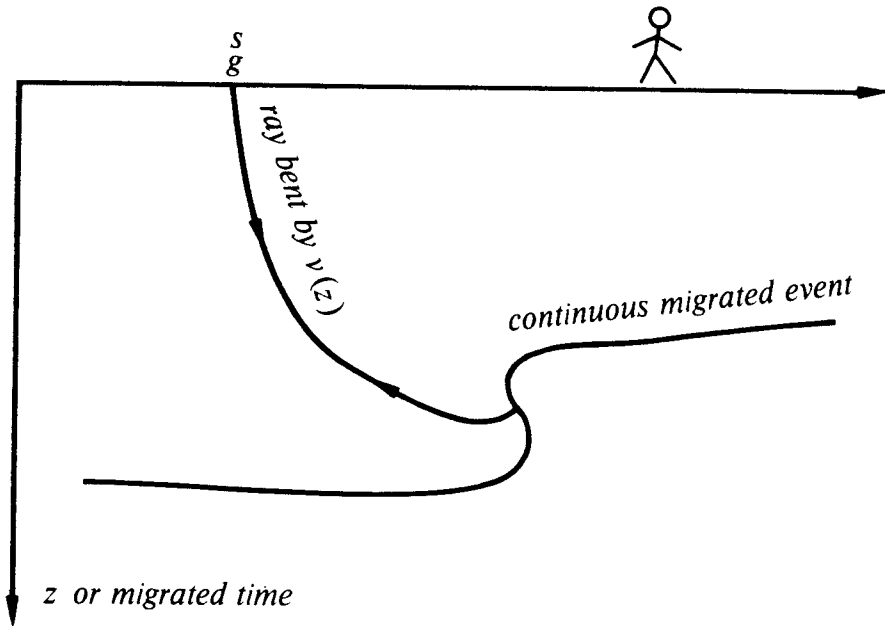


FIG. 4.2-7. Ray reflected from the underside of an overthrust.

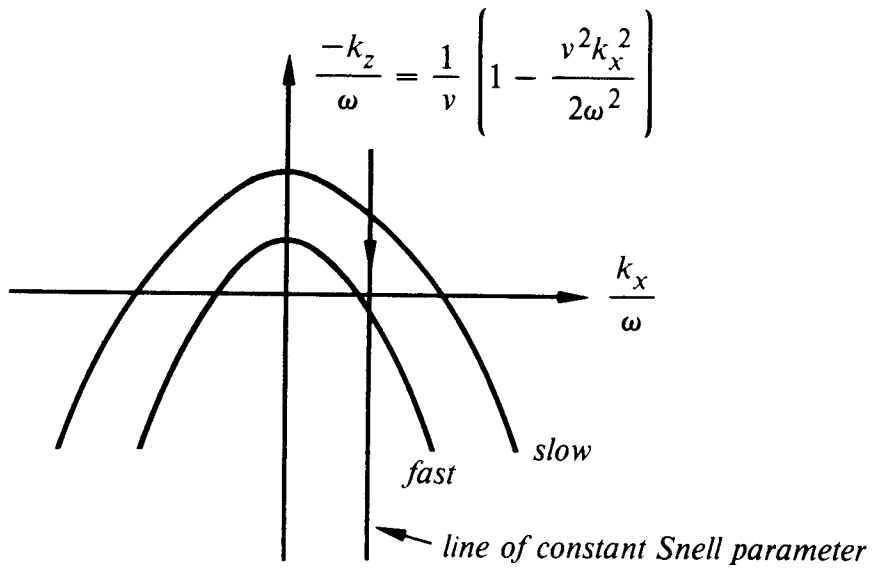


FIG. 4.2-8. Dispersion curve at two different velocities,  $v_{fast}$  and  $v_{slow}$ .

dispersion curve. But as deeper velocity material is encountered, that same stepout implies a negative phase velocity. Although the thrust angle is unlikely to be quantitatively correct, the general picture is appropriate. It is like figure 6. If you want a quantitatively correct migration, see Section 4.5, or for something completely different, see the method of Kosloff et al. [1983] and Baysal et al. [1983].

### Analyzing Errors of Migration

A dipping reflector that is flat and regular can be analyzed in its entirety using the phase velocity concept. The group velocity concept is required only when more than one angle is simultaneously present. This simultaneity occurs with the point scatterer response. It also occurs when there is variable reflection amplitude along a dipping bed. The group velocity is needed because representation of either a curved event or an amplitude anomaly requires a range of plane-wave angles. Analogously, in time-series analysis the Fourier representation of an amplitude-modulated sinusoid requires a bandwidth of sinusoids.

Figure 9 depicts a smooth, flat, dipping bed that has been undermigrated because the  $\hat{k}_z$  defined by some rational square-root approximation or some numerical approximation did not match the correct square-root value of  $k_z$ .

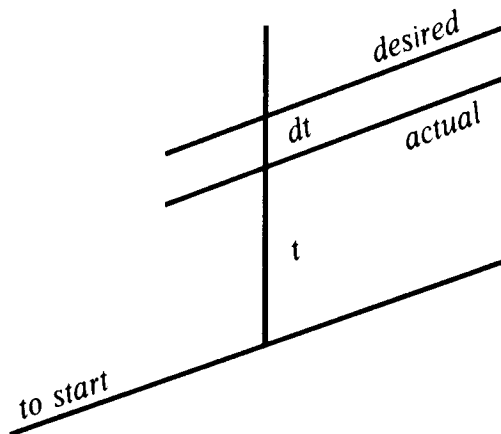


FIG. 4.2-9. Undermigrated dipping reflector.



The error in figure 9 is entirely a time-shift error. Since the reflection coefficient is constant along the reflector, no lateral shift error can be recognized. The time error may be theoretically determined by

$$\frac{dt}{t} \approx \frac{dz}{z} \approx \frac{\hat{k}_z - k_z}{k_z} \quad (2)$$

For the so-called 15° equation, it turns out that about a half-percent phase error is made at 25°.

Next, the error in the collapse of a hyperbola will be determined. Figure 10 depicts the downward continuation of a hyperbola. For clarity, the downward continuation was not taken all the way to the focus. Select a ray of some Snell's parameter  $p = dt/dx$  by choosing some slope  $p$ . Imagine a tangent line segment of slope  $p$  to each of the hyperboloids. If there were a little amplitude anomaly where the slope is  $p$ , you would be able to identify it on each of the hyperboloids.

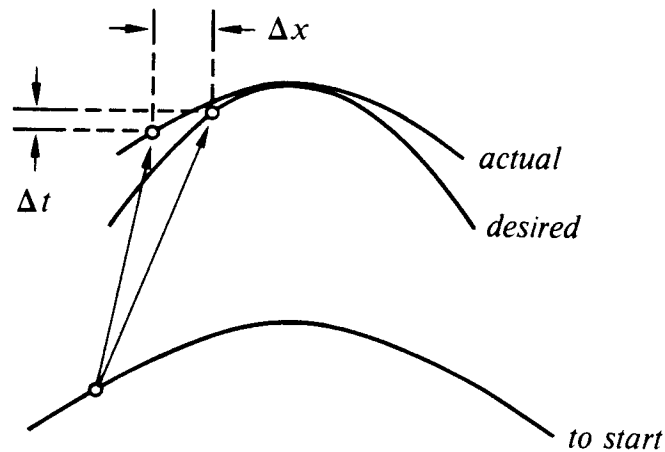


FIG. 4.2-10. Error of hyperbola collapse. Note that the actual curve is above the desired curve, but the actual point is below the desired point.

In figure 10 the amount of time moved is too little; likewise, the lateral distance moved is too small. In practice, errors of the 15° equation with  $r_0 = 1$  are sometimes compensated by an increase in either  $z$  or  $v$  of about 6%. The amounts of the errors may be calculated from

$$\frac{\Delta t}{t} = \frac{\frac{\partial}{\partial \omega} (\hat{k}_z - k_z)}{\frac{\partial}{\partial \omega} k_z} \quad (3a)$$

$$\frac{\Delta x}{x} = \frac{\frac{\partial}{\partial k_x} (\hat{k}_z - k_z)}{\frac{\partial}{\partial k_x} k_z} \quad (3b)$$

where  $k_z$  is taken to be a function of  $\omega$  and  $k_x$ . It turns out that for the 15° equation, about a half-percent group velocity error occurs at 20°. Thus the group velocity error is generally worse than the phase velocity error.

### Derivation of Group Velocity Equation

An impulse function at the origin in  $(x, z)$ -space is a superposition of Fourier components:

$$\iint e^{+i k_x x + i k_z z} dk_x dk_z \quad (4)$$

Physics (and perhaps numerical analysis) leads to a dispersion relation that is a functional relation between  $\omega$ ,  $k_x$ , and  $k_z$ , say,  $\omega(k_x, k_z)$ . The most common example of such a dispersion relation is the scalar wave equation  $\omega^2 = v^2 (k_x^2 + k_z^2)$ . The solution to the equation is

$$e^{-i \omega t + i k_x x + i k_z z} \quad (5)$$

Integrating (5) over  $(k_x, k_z)$  produces a monochromatic time function that at  $t=0$  is an impulse at  $(x, z)=(0, 0)$ . This expression at some very large time  $t$  is

$$\iint e^{-i t [\omega(k_x, k_z) - k_x x/t - k_z z/t]} dk_x dk_z \quad (6)$$

At  $t$  very large, the integrand is a very rapidly oscillating function of unit magnitude. Thus the integral will be nearly zero unless the quantity in square brackets is found to be nearly independent of  $k_x$  and  $k_z$  for some sizable area in  $(k_x, k_z)$ -space. Such a flat spot can be found in the same way that the maximum or minimum of any two dimensional function is found, by setting derivatives equal to zero. This analytical approach is known as the stationary phase method. It gives

$$0 = \frac{\partial}{\partial k_x} [ \quad ] = \frac{\partial \omega}{\partial k_x} - \frac{x}{t} \quad (7a)$$

$$0 = \frac{\partial}{\partial k_z} [ \quad ] = \frac{\partial \omega}{\partial k_z} - \frac{z}{t} \quad (7b)$$

So, in conclusion, at time  $t$  the disturbances will be located at

$$(x, z) = t \left( \frac{\partial \omega}{\partial k_x}, \frac{\partial \omega}{\partial k_z} \right) \quad (8)$$

which justifies the definition of group velocity.

Now let us see how figure 2a was calculated. The 15° dispersion relation was solved for  $\omega$  and inserted into (8). The resulting  $(x, z)$  turned out to be a function of  $k_x/\omega$ . Trying all possible values of  $k_x/\omega$  gave the curve.

### Derivation of Energy Migration Equation

Energy migration in  $(x, t)$ -space is analyzed in a fashion similar to the way the group velocity was derived. Take depth to be large in the integral

$$\iint e^{i z [k_z(\omega, k_x) - \omega t/z + k_x x/z]} d\omega dk_x \quad (9)$$

The result is that the energy goes to

$$(x, t) = z \left( -\frac{\partial k_z}{\partial k_x}, \frac{\partial k_z}{\partial \omega} \right) \quad (10)$$

This justifies our previous assertion that (3) can be used to analyze energy propagation errors. Equation (10) was also used to calculate the curve in figure 3. The validity of the stationary phase concept is confirmed by figure 4, which was produced using inverse Fourier transformation.

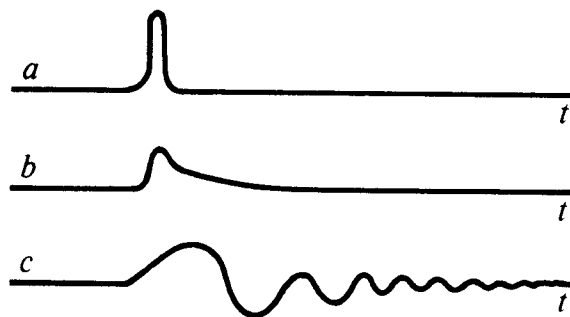
### Extrapolation Equations are not Frequency-Dispersive.

To prove that the familiar 15°, 45°, etc. wave extrapolators are not frequency-dispersive, recall from Section 2.2 that the dispersion relations all have the form  $k_z/\omega = f(k_x/\omega)$ , where  $f$  is a semicircle approximation, say, 15° or 45°. No dispersion relation of this form can be frequency-dispersive. Performing the derivatives required by (10), you see that while the  $(x, t)$ -coordinates of a wavefront depend on the dip angle through the parameter  $vk_x/\omega$ , they do not depend explicitly on  $\omega$ . So any frequency dispersion observed in practice does not arise from a 15° or 45° approximation.

### 4.3 Frequency Dispersion and Wave-Migration Accuracy

Frequency dispersion results from different frequencies propagating at different speeds. The physical phenomenon of frequency dispersion is rarely heard in daily life, although many readers may have heard it while ice skating on lakes and rivers. Elastic waves caused by cracking ice propagate dispersively, causing pops to change into percussive notes. Frequency dispersion is generally observable on seismic waves that propagate along the earth's surface but frequency dispersion is hardly ever perceptible on internally reflected waves. In seismic data processing, frequency dispersion is a nuisance and an embarrassment to process designers. It arises mainly with the finite differencing method because differential operators and difference operators do not coincide at high frequencies. Frequency dispersion can always be suppressed by sampling more densely, and it is the job of the production analyst to see that this is done. Figure 1 depicts some dispersed pulses.

FIG. 4.3-1. (a) A pulse. (b) A pulse slightly dispersed as by the physical dissipation of high frequencies. (c) A pulse with a substantial amount of frequency dispersion, such as could result from careless data processing.



Frequency dispersion caused by data processing can be a useful warning that the data is in danger of being aliased. Frequency-domain methods do not depend on difference operators, so they have the advantage of not showing dispersion. The penalties that go along with this advantage are (1) limitation to constant material properties, (2) wraparound, and (3) the occurrence of spatial aliasing without the warning of dispersion.

Figure 2 shows an example of frequency dispersion in migrated data. At the top of the figure is a CDP stack. In the middle is the data after

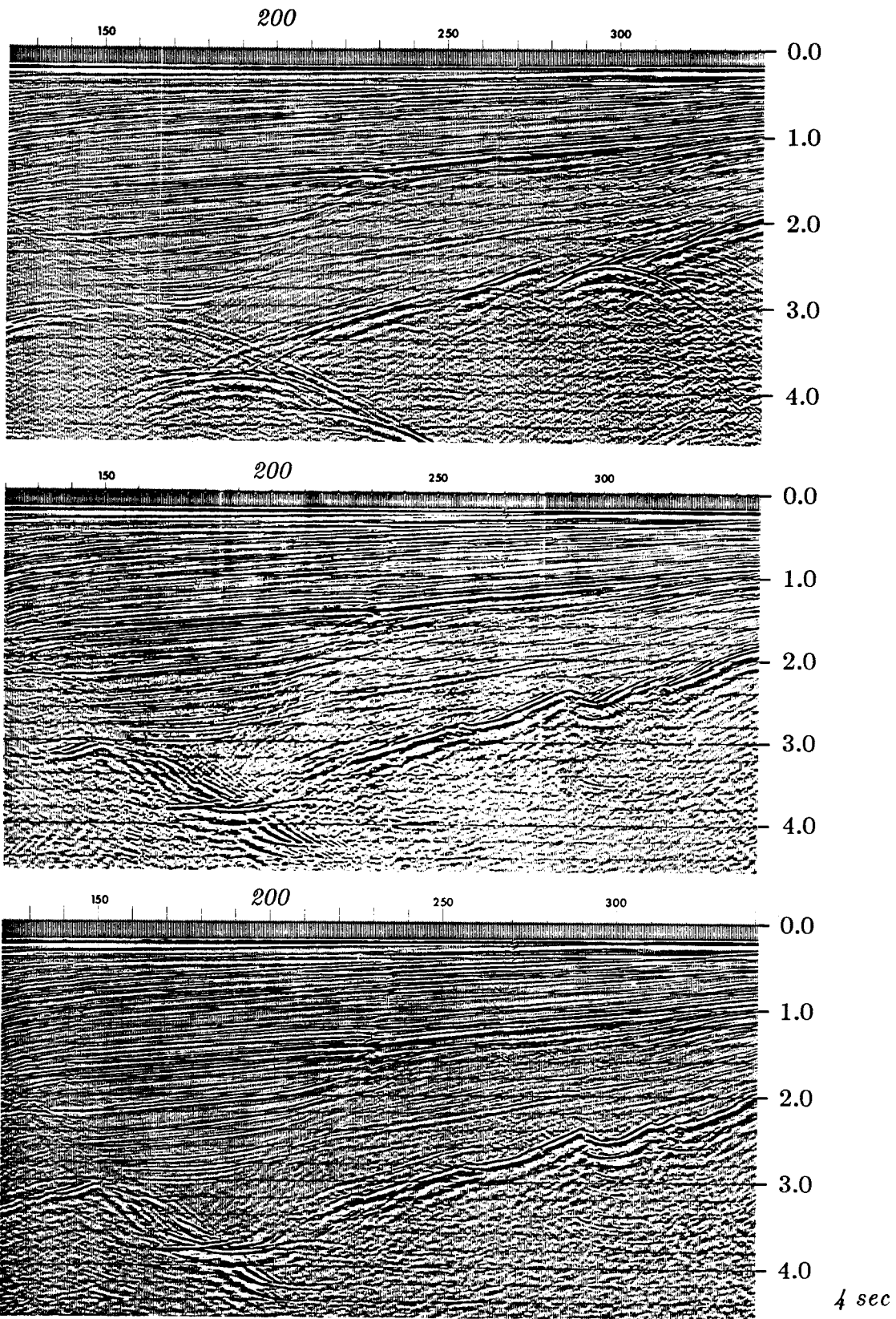


FIG. 4.3-2. Conquering frequency dispersion. (Taner and Koehler, distributed by Seiscom Delta Inc.)

processing with no attempt to control frequency dispersion. The worst dispersion is near shot point 200 at 4 seconds. The bottom shows the data after reprocessing with greater attention to dispersion.

### Spatial Aliasing

Aliasing can occur on the axes of time, depth, geophone, shot, midpoint, offset, or crossline. Aliasing is the worst on the horizontal space axes. Section 1.3, figure 3 provides an illustration. Looking at that figure, you get confused about whether the dip is to the left or right. Mathematical analysis has the same difficulty. The dispersion relation of the wave equation enables us to compute the vertical spatial frequency  $k_z$  from the temporal frequency  $\omega$ , the velocity  $v$ , and the horizontal spatial frequency  $k_x$  using the semicircle relation  $k_z(\omega, k_x) = \sqrt{\omega^2/v^2 - k_x^2}$ . Sampling on the  $x$ -axis sets an upper limit on  $k_x$  equal to the Nyquist frequency  $\pi/\Delta x$ . Both frequency-domain methods and finite-difference methods treat higher frequencies as though they were folded back at the Nyquist frequency. Thus the semicircle dispersion relation is replicated above the Nyquist frequency, as shown in figure 3.

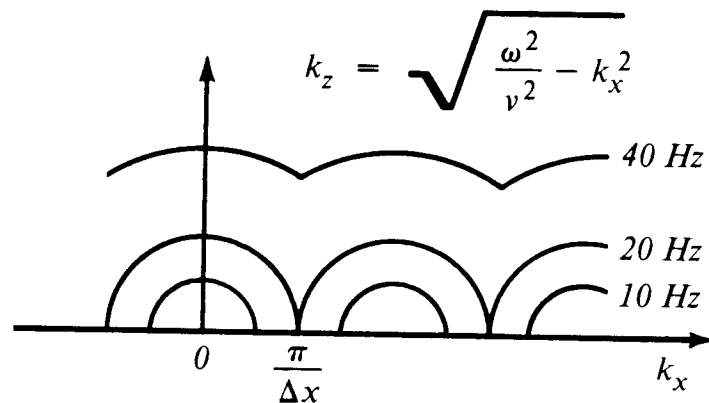


FIG. 4.3-3. The effective dispersion relation of the wave equation when the horizontal axis is sampled. Frequencies are given for typical zero-offset migration.

The problem of spatial aliasing begins when two circles touch each other, as shown at 20 Hz in figure 3. This occurs when a half-wavelength  $v/2f$  equals the spatial sample rate  $\Delta x$ . The exploding-reflector model implies that the velocity to use is half the rock velocity. Thus the aliasing problem is avoided if  $2f \Delta x < 1/2 v_{rock}$ . For a rock velocity equal to 2 km/sec, the

safe frequencies are listed in the table below:

	$\Delta x$	<i>safe frequency</i>
<i>standard</i>	25 m	< 20 Hz
<i>reconnaissance</i>	50 m	< 10 Hz
<i>3-D cross line</i>	100 m	< 5 Hz

Another view of the spatial aliasing problem is that steeply dipping waves are suppressed by the geophone group. (This disregards shot-space aliasing). From this standpoint the limit past which spatial aliasing begins should be thought of in terms of angles at which energy is missing from the data. Taking the ray angle to be 30° instead of 90° doubles horizontal wavelengths. Thus, for 30° and a rock velocity of 2 km/sec, to ensure safety from aliasing, frequencies should be in the ranges listed below:

	$\Delta x$	<i>safe frequency</i>
<i>standard</i>	25 m	< 40 Hz
<i>reconnaissance</i>	50 m	< 20 Hz
<i>3-D cross line</i>	100 m	< 10 Hz

Because data usually has good signal above 40 Hz, wide-angle processing is often frustrated by spatial aliasing.

The problem of spatial aliasing usually overshadows the difference between the 15° and the 90° equations. Aliased energy does not move between hyperbola flanks and the apex. Aliased energy tends to stay in place. This is illustrated on figure 4 which shows a 90° hyperbola and a 15° hyperboloid from a finite difference equation. Overall, there is little difference. Look at the amplitude of the hyperbolic arrival. It is dropping off faster than predicted by spherical spreading and the obliquity function. This is because the dispersion curve semicircles overlap one another. There can be no angles of propagation beyond that which aliases  $x$ . Since waves can't go so steeply, they don't. The pulse doesn't spread properly.

### Second Space Derivatives

The defining equation for a second *difference* operator is

$$\frac{\delta^2}{\delta x^2} P = \frac{P(x + \Delta x) - 2P(x) + P(x - \Delta x)}{(\Delta x)^2} \quad (1)$$

The second *derivative* operator is defined by taking the limit

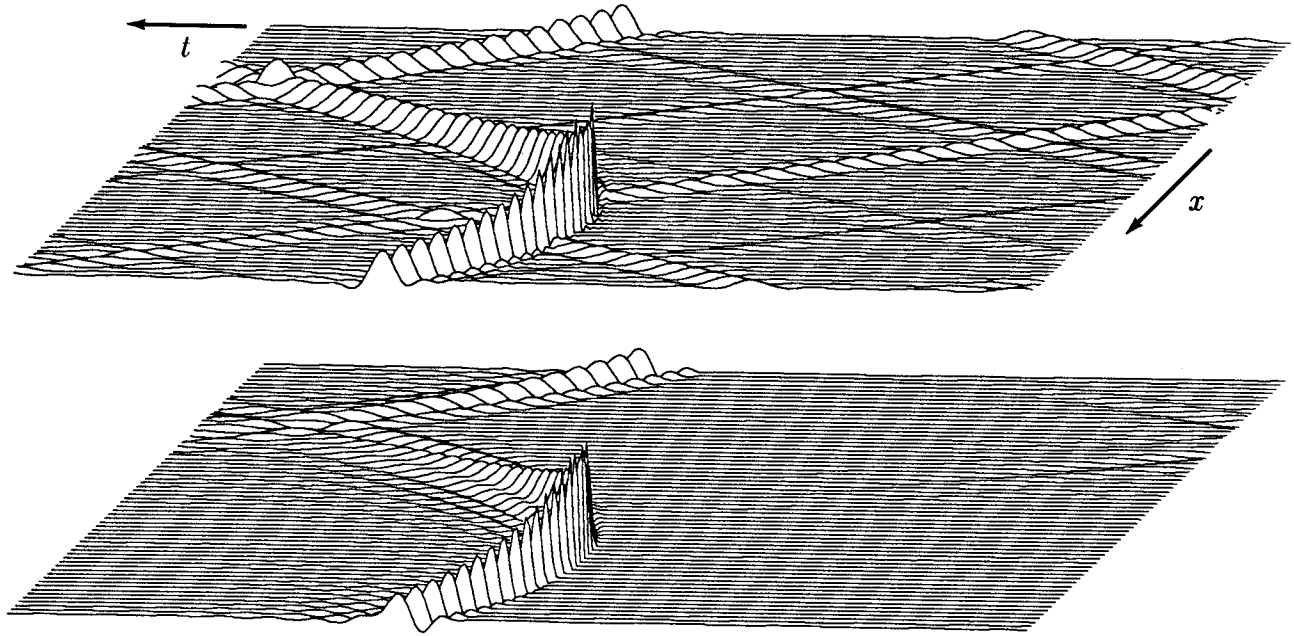


FIG. 4.3-4. One second of synthetic hyperbolas with  $\Delta t = 4$  ms,  $\Delta x = 25$  meters, and velocity 2 km/sec. Fourier domain  $90^\circ$  hyperbola (top) and  $15^\circ$  finite difference hyperboloid (bottom).

$$\frac{\partial^2}{\partial x^2} P \quad \lim_{\Delta x \rightarrow 0} = \frac{\delta^2}{\delta x^2} P \quad (2)$$

Many different definitions can all go to the same limit as  $\Delta x$  goes to zero. The problem is to find an expression that is accurate when  $\Delta x$  is larger than zero and, on a practical level, is not too complicated. Our first objective is to see how the accuracy of equation (1) can be evaluated quantitatively. Second, we will look at an expression that is slightly more complicated than (1) but much more accurate.

The basic method of analysis we will use is Fourier transformation. Take the derivatives of the complex exponential  $P = P_0 \exp(ikx)$  and look at any errors as functions of the spatial frequency  $k$ . For the second derivative,

$$\frac{\partial^2}{\partial x^2} P = -k^2 P \quad (3)$$

Define  $\hat{k}$  by an expression analogous to the difference operator:

$$\frac{\delta^2}{\delta x^2} P = -\hat{k}^2 P \quad (4)$$



Ideally  $\hat{k}$  would equal  $k$ . Inserting the complex exponential  $P = P_0 \exp(ikx)$  into (1), we see that the definition (4) gives an expression for  $\hat{k}$  in terms of  $k$ :

$$-\hat{k}^2 P = \frac{P_0}{\Delta x^2} \left[ e^{ik(x+\Delta x)} - 2e^{ikx} + e^{ik(x-\Delta x)} \right] \quad (5a)$$

$$-\frac{\delta^2}{\delta x^2} = \hat{k}^2 = \frac{2}{\Delta x^2} [1 - \cos(k \Delta x)] \quad (5b)$$

It is a straightforward matter to make plots of  $\hat{k} \Delta x$  versus  $k \Delta x$  from (5b). The half-angle trig formula allows us to take an analytic square root of (5b), which is

$$\frac{\hat{k} \Delta x}{2} = \sin \frac{k \Delta x}{2} \quad (5c)$$

Series expansion shows that for low frequencies  $\hat{k}$  is a good approximation to  $k$ . At the Nyquist frequency, defined by  $k \Delta x = \pi$ , the approximation  $\hat{k} \Delta x = 2$  is a poor approximation to  $\pi$ .

### The 1/6 Trick

Increased absolute accuracy may always be purchased by reducing  $\Delta x$ . Increased accuracy relative to the Nyquist frequency may be purchased at a cost of computer time and analytical clumsiness by adding higher-order terms, say,

$$\frac{\partial^2}{\partial x^2} \approx \frac{\delta^2}{\delta x^2} - \frac{\Delta x^2}{12} \frac{\delta^4}{\delta x^4} + \text{etc.} \quad (6)$$

As  $\Delta x$  tends to zero (6) tends to the basic definitions (1) and (2). Coefficients like the 1/12 in (6) may be determined by the Taylor-series method if great accuracy is desired at small  $k$ . Or somewhat different coefficients may be determined by curve-fitting techniques if accuracy is desired over some range of  $k$ . In practice (6) is hardly ever used, because there is a less obvious expression that offers much more accuracy at less cost! The idea is indicated by

$$\frac{\partial^2}{\partial x^2} \approx \frac{\frac{\delta^2}{\delta x^2}}{1 + b \Delta x^2 \frac{\delta^2}{\delta x^2}} \quad (7a)$$

where  $b$  is an adjustable constant. The accuracy of (7a) may be numerically

evaluated by substituting from (5b) to get

$$\left( \frac{\hat{k} \Delta x}{2} \right)^2 = \frac{\sin^2 \frac{k \Delta x}{2}}{1 - b \ 4 \sin^2 \frac{k \Delta x}{2}} \quad (7b)$$

The square root of (7b) is plotted in figure 5 for a value of  $b = 1/6$ .

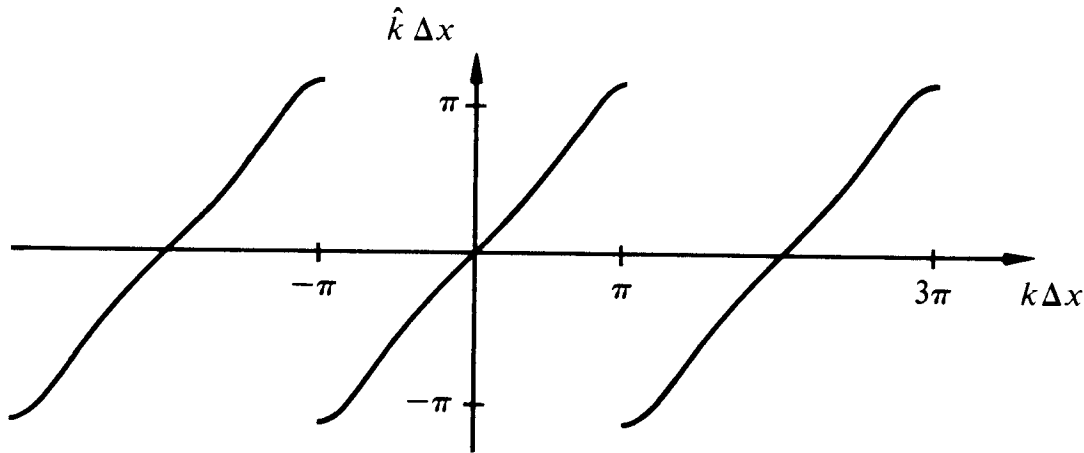


FIG. 4.3-5. Accuracy of the second-derivative representation (7) (for  $b = 1/6$ ) as a function of spatial wavenumber. The sign of the square root of (7b) was chosen to agree with  $k$  in the range  $-\pi$  to  $\pi$  and to be periodic outside the range. (Hale)

Taking  $b$  in (7) to be  $1/12$ , then (7) and (6) would agree to second order in  $\Delta x$ . The  $1/12$  comes from series expansion, but the  $1/6$  fits over a wider range and is a value in common use. Francis Muir has pointed out that the value  $1/4 - 1/\pi^2 \approx 1/6.726$  gives an *exact* fit at the Nyquist frequency and an accurate fit over all lower frequencies! Few explorationists consider the remaining accuracy deficiency of (7) to be sufficient to warrant interpolation of field-recorded values. Figure 6 compares hyperbolas for various values of  $b$ . Observe in figure 6 that the longest wavelengths travel at the same speed regardless of  $b$ . The time axis in figure 6 is only 256 points long, whereas in practice it would be a thousand or more. So figure 6 exaggerates the frequency dispersion attributable in practice to finite differencing the  $x$ -axis.

Let us be sure it is clear how (7) is put into use. Take  $b = 1/6$ . The simplest prototype equation is the heat-flow equation:

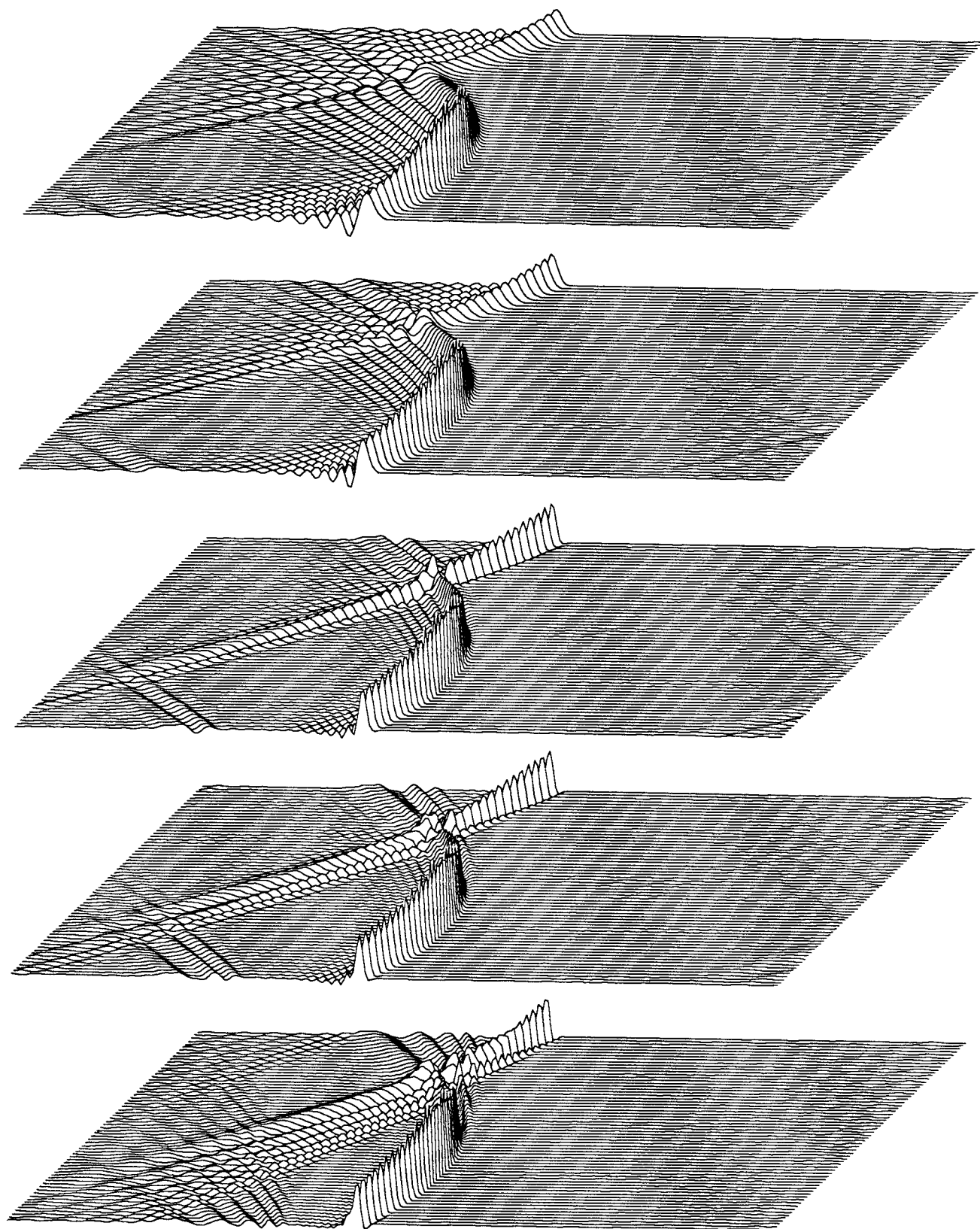


FIG. 4.3-6. Hyperbolas for  $b = 0, 1/12, 1/6.726, 1/6, 1/5$ .

$$\frac{\partial}{\partial t} q = \frac{\partial^2}{\partial x^2} q \approx \frac{\frac{\delta^2}{\delta x^2}}{1 + \frac{\Delta x^2}{6} \frac{\delta^2}{\delta x^2}} q \quad (8)$$

Multiply through the denominator:

$$\left( 1 + \frac{\Delta x^2}{6} \frac{\delta^2}{\delta x^2} \right) \frac{\partial}{\partial t} q \approx \delta_{xx} q \quad (9)$$

### Time and Depth Derivatives — the Bilinear Transform

You might be inclined to think a second derivative is a second derivative and that there is no mathematical reason to do time derivatives differently than space derivatives. This is not the case. A hint of disparity between  $t$  and  $x$  derivatives comes from boundary conditions. With time derivatives (and often with the depth  $z$  derivative) we must consider causality — which means the future is determined solely from the present and past. Appropriate boundary conditions on the time axis are initial conditions — the function (and perhaps some derivatives) is specified at *one* point, the initial point in time. For depth  $z$  that special point is the earth's surface at  $z=0$ . But lateral space derivatives are different: they require boundary conditions at two widely separated points, usually at the left and right sides of the volume.

The differential equation

$$\frac{dq}{dz} = i k_z(\omega, k_x) q \quad (10)$$

is associated with the very definition of  $k_z$ . The analogous difference equation will define  $\hat{k}_z$ :

$$\frac{q_{z+\Delta z} - q_z}{\Delta z} = i \hat{k}_z \frac{q_{z+\Delta z} + q_z}{2} \quad (11)$$

Inserting the solution of (10)  $q = q_0 \exp(ik_z z)$  into (11) gives us the relation between the desired  $k_z$  and the actual  $\hat{k}_z$ .

$$i \hat{k}_z \Delta z = 2 \frac{e^{ik_z \Delta z} - 1}{e^{ik_z \Delta z} + 1} = 2 \frac{e^{ik_z \Delta z/2} - e^{-ik_z \Delta z/2}}{e^{ik_z \Delta z/2} + e^{-ik_z \Delta z/2}} \quad (12)$$

This equation is known as the bilinear transform (Section 4.6).

$$i \hat{k}_z \Delta z = 2i \frac{\sin k_z \Delta z/2}{\cos k_z \Delta z/2} \quad (13)$$

$$\frac{\hat{k}_z \Delta z}{2} = \tan \frac{k_z \Delta z}{2} \quad (14)$$

Equation (14) gives the accuracy of first derivatives obtained using the Crank-Nicolson method. Recall the migration differencing schemes in Section 2.7. We did the time differencing in the same way that we did the depth differencing. So the same accuracy limitation must apply, namely,

$$\frac{\hat{\omega} \Delta t}{2} = \tan \frac{\omega \Delta t}{2} \quad (15)$$

Series expansion shows that  $\hat{\omega}$  goes to  $\omega$  as  $\Delta t$  goes to zero. Relative errors in  $\omega$  at (4, 10, and 20) points per wavelength are (30%, 3%, and 1%). These errors are quite large, calling for either a choice of small  $\Delta t$  or a more accurate method than (14).

The bad news is that there does not seem to exist a representation of causal differentiation that is any more accurate than the Crank-Nicolson representation. There is nothing like the 1/6 trick. Thus the sample intervals of  $\Delta z$  and  $\Delta t$  must be reduced considerably from the Nyquist criterion. The practical picture may not be as bleak as the one I am painting. Many people are pleased with both the speed and accuracy of time-domain migrations at  $\Delta t = 4$  milliseconds.

Stolt's classic paper [1978] besides introducing the fast Fourier transform migration method, points out that more accuracy can be achieved when the requirement of causality is dropped. Stolt shows how dropping causality at the known depth level while retaining it at the next level allows stable finite differencing. With the depth  $z$ -axis we are stuck with causal derivatives, although Fourier methods could be used for discrete layers. The depth axis is not so troublesome as the  $x$ - and  $t$ -axes, however, because it affects computer time only, not data storage.

Finite difference solutions don't just approximate the frequency — what they really do is to approximate  $\exp ik_z \Delta z$ . Solve (11) for the unknown.

$$q_{z+\Delta z} = \left( \frac{1 + i \hat{k}_z \Delta z / 2}{1 - i \hat{k}_z \Delta z / 2} \right) q_z \quad (16)$$

So for  $N_z$  layers in depth  $z = N \Delta z$  we have the approximation

$$e^{ik_z N \Delta z} \approx \left( \frac{1 + i \hat{k}_z \Delta z / 2}{1 - i \hat{k}_z \Delta z / 2} \right)^N \quad (17)$$

which will be of later use for Fourier domain simulations of finite difference

programs. Such simulations, coming in Section 4.7, enable us to compare the accuracy of various migration methods.

## 4.4 Absorbing Sides

Computer memory cells are often used to model points in a volume that contains propagating waves. Though we often wish to model an infinite volume, the number of computer cells is, regrettably, finite. Waves in the computer reflect back from the boundaries of the finite computer memory when we would prefer that the waves had gone away to infinity. To avoid the need for infinite computer capacity this section develops the theory of absorptive side boundary conditions.

There are two kinds of side boundary difficulties. First is where we are at the end of our observations. Second is where we somehow decided to limit the extent of our calculations. These boundaries might be the same. But to avoid confusion, let us presume that the data is of more limited extent than the computer memory. So alongside the data, which comprises the initial conditions for the calculation, is a region which will be called the *data padding*.

### Data Padding

The crudest assumption is that additional zero-valued data may be presumed for the padded area. To avoid an edge diffraction artifact the data must merge smoothly with the padding. So zero padding is a good assumption only if the data is already small around the side boundary. When data is zero padded, it is debatable whether or not it should be tapered (gradually scaled to zero) to match up smoothly with the zero padding. I prefer to avoid tapering the data. That amounts to falsifying it. Instead I prefer to pad the data not with zeroes, but with something that looks more like the data. A simple way is to replicate the last trace, scaling it downward with distance from the boundary. This works best when the stepout of the data matches the stepout of the extension. Any theory for optimum data padding has two

important ingredients: a noise model and a signal model. An ideal data extrapolation is rarely, if ever, available in practice. Section 3.5 contains suggestions for more elaborate models for extensions of gathers.

### Truncation at Cable Ends and at Survey Ends

In exploration there are two kinds of horizontal truncation problems. The first, which is at the end of the geophone cable, affects mainly common-midpoint stacking. The second is at the geographical boundaries of the survey and affects mainly migration. In both migration and stacking, hyperboloids are collapsed to points. But the processes differ because of the data itself. With stacking, it is predictable that energy will dip downward toward the far-offset cable truncation. With migration, reflectors can dip either downward or upward at the ends of the section. The downward-dipping case is better behaved. There seismic events move smoothly from the boundary to the interior.

The troublesome case occurs with migration when the seismic events dip upward at the edges of the survey. Then downward continuation moves seismic energy toward the boundary. On arriving at the boundary, it bounces back with opposite dip, and interferes with energy still moving toward the boundary. The problem may be reduced by appending space to the sides of the dataset, thus providing the dipping energy with a place to go. (You have previously decided what initial data padding to put in this space).

### Engquist Boundaries for the Scalar Wave Equation

The simplest “textbook” boundary condition is that a function should vanish on the boundary. A wave incident onto such a boundary reflects with a change in polarity (so that the incident wave plus the reflected wave will vanish on the boundary). The next-to-simplest boundary condition is the zero-slope condition. It is also a perfect reflector, but the reflection coefficient is  $+1$  instead of  $-1$ . Two points at the edge of the differencing mesh are required to represent the zero-slope boundary. The most general boundary condition usually considered is a linear combination of function value and slope. This is also a two-point boundary condition. It so happens that our extrapolation equations (Section 2.2) contain only a single depth derivative, so that on the  $z$ -axis they are a two-point condition. Observing this, Björn Engquist recognized a new application for our extrapolation equations. Many researchers in other disciplines are interested in forward modeling, that is, evolving forward in time with an equation like the scalar wave equation, say,  $P_{xx} + P_{zz} = P_{tt}/v^2$ . These people suffer severely the consequences of

limited memory. Engquist's idea was that they should use our extrapolation equations for their boundary conditions. (This idea led to his winning the SIAM prize). Suppose they desire an infinite absorbing volume surrounding a box in the  $(x, z)$ -plane. Then they need a boundary condition that goes all the way around the box. They could use the downgoing wave equation on the bottom of the box and the upcoming wave equation on the top edge. The sides could be handled analogously with an interchange of  $x$  and  $z$ . This idea was thoroughly tested and confirmed by Robert Clayton. For an example of one of his comparisons, see figure 1.

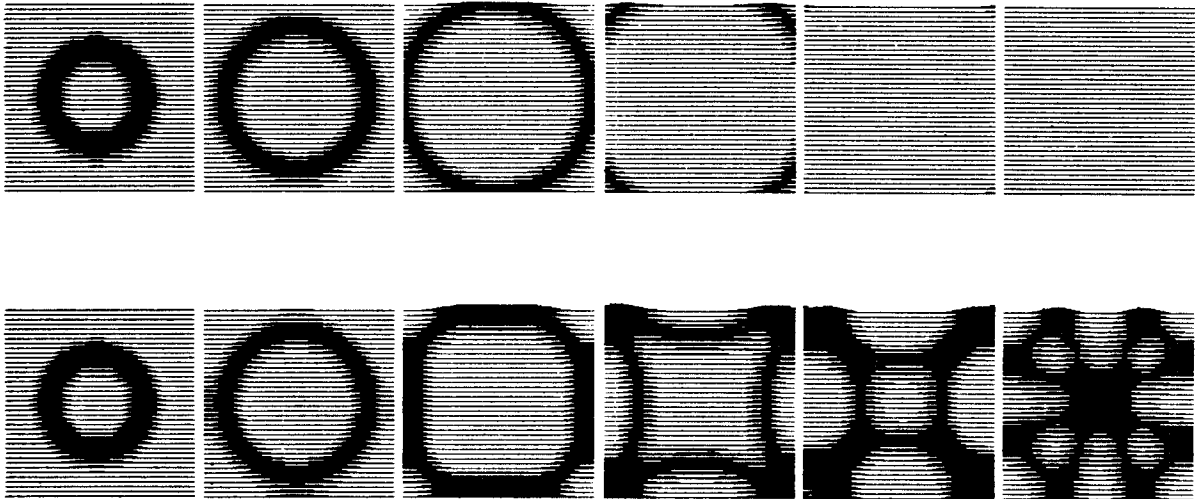


FIG. 4.4-1. Expanding circular wavefront in a box with absorbing sides (top) and zero-slope sides (bottom). (Clayton)

### Engquist Side Conditions for the Extrapolation Equations

In data processing an extrapolation equation is used in the interior of the region under study. This is unlike forward modeling, in which the full scalar wave equation is used in the interior and an extrapolation equation can be used on the boundary. The scalar wave equation has a circular dispersion relation, whereas the extrapolation equation has, ideally, a semicircular one. Reasoning by analogy, Engquist speculated that a quarter-circular dispersion relation might be an ideal side boundary for wave-extrapolation problems. To make his idea more specific and immediately applicable, he proposed that the quarter-circle be approximated by a straight line. This is shown in figure 2.

The advantage of the straight-line dispersion relation is that in the space domain it is represented by a simple, first-order, differential equation. A



first-order equation has first derivatives that can be expressed over just two data points, and thus it can be used as a conventional, two-point, side-boundary condition. The right-side equation in figure 2 defines the boundary dispersion relation  $D$ :

$$0 = \frac{vk_z}{\omega} - 1 + \text{const} \frac{k_x}{\omega} = D(\omega, k_x, k_z) \quad (1)$$

In  $(t, x, z)$ -space this equation is

$$0 = \left( v \frac{\partial}{\partial z} + \frac{\partial}{\partial t} + \text{const} \frac{\partial}{\partial x} \right) P \quad (2)$$

In retarded time,  $\partial/\partial z$  may be eliminated by substitution from the interior equation.

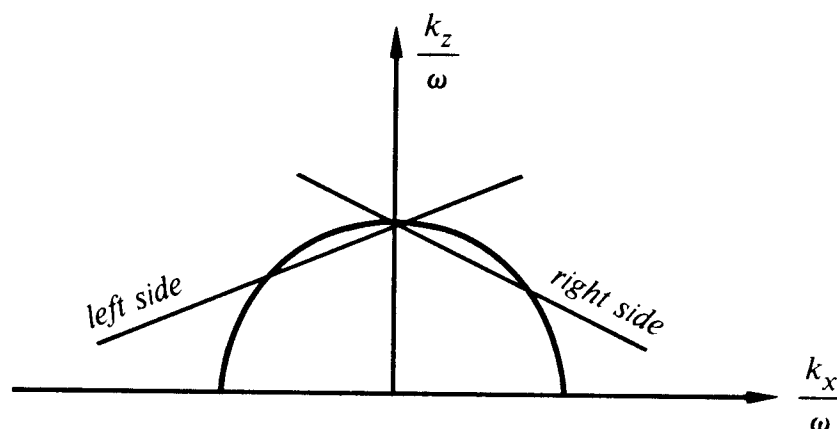


FIG. 4.4-2. Dispersion relation of simple absorbing side conditions.

For a mathematical, nonphysical point of view, imagine some peculiar physics which prescribe that the physical equation that applies in some region is just the equation which has the dispersion relation of the absorbing side condition. Beside this fictitious region imagine another in which the usual extrapolation equation applies. At the point of contact between the regions the solutions would match. It may come as no great surprise that the smallest boundary reflections would occur where the two dispersion relations were a good match to each other. So the slope of the straight line would be selected to form a good fit over the range of angles of interest. An example of side-boundary absorption during migration is shown in figure 3.

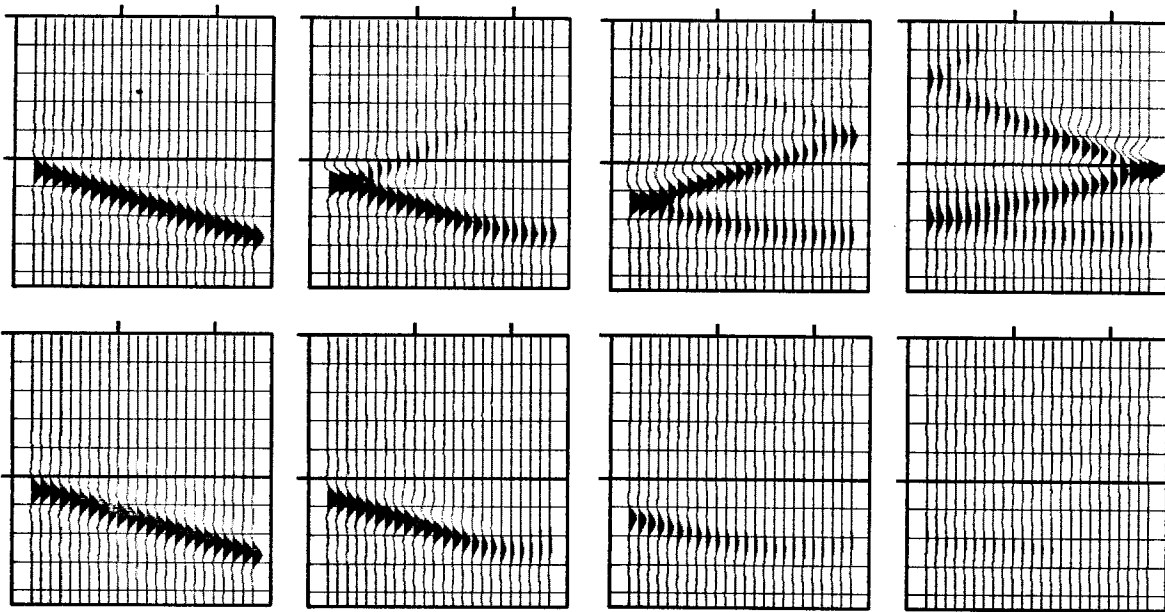


FIG. 4.4-3. Downward continuation with zero slope side boundaries (top), and absorbing side boundaries (bottom). (Toldi)

### Size of the Reflection Coefficient

Let us look at some of the details of the reflection coefficient calculation. A unit amplitude, monochromatic plane wave incident on the side boundary generates a reflected wave of magnitude  $c$ . The mathematical representation is:

$$P(x, z) = e^{-i\omega t + i k_z z} \left( e^{+i k_x x} + c e^{-i k_x x} \right) \quad (3)$$

In equation (3)  $\omega$  and  $k_x$  are arbitrary, and  $k_z$  is determined from  $\omega$  and  $k_x$  using the dispersion relation of the *interior* region, i.e., a semicircle approximation. Assuming this interior solution is applicable at the side boundary, you insert equation (3) into the differential equation (2), which represents the side boundary. As a result,  $\partial/\partial x$  is converted to  $+i k_x$  on the incident wave, and  $\partial/\partial x$  is converted to  $-i k_x$  on the reflected wave. Also,  $\partial/\partial z$  is converted to  $i k_z$ . Thus the first term in (3) produces the dispersion relation  $D(\omega, k_x, k_z)$  times the amplitude  $P$ . The second term produces the reflection coefficient  $c$  times  $D(\omega, -k_x, k_z)$  times  $P$ . So (2) with (3) inserted becomes:

$$c = \frac{-D(\omega, k_x, k_z)}{D(\omega, -k_x, k_z)} \quad (4)$$

The case of zero reflection arises when the numerical value of  $k_z$  selected by the interior equation at  $(\omega, k_x)$  happens also to satisfy exactly the dispersion relation  $D$  of the side boundary condition. This explains why we try to match the quarter-circle as closely as possible. The straight-line dispersion relation does *not* correspond to the most general form of a side boundary condition, which is expressible on just two end points. A more general expression with adjustable parameters  $b_1$ ,  $b_2$ , and  $b_3$ , which fits even better, is

$$D(\omega, k_x, k_z) = \left( 1 - b_3 \frac{vk_x}{\omega} \right) \frac{vk_z}{\omega} - \left( b_1 - b_2 \frac{vk_x}{\omega} \right)$$

The absolute stability of straight-line absorbing side boundaries for the 15° equation can be established, including the discretization of the  $x$ -axis. Unfortunately, an airtight analysis of stability seems to be outside the framework of the Muir impedance rules. As a consequence, I don't believe that stability has been established for the 45° equation.

## 4.5 Tuning up Fourier Migrations

First we will see how to migrate dips greater than 90°. Then we will attack the main two disadvantages of Fourier migrations, namely, their periodicity and their poor tolerance of space-variable velocity.

### Dips Greater than 90°

Migration of dips greater than 90° requires careful handling of evanescent energy. As this is being written, most migration-by-depth-extrapolation programs ignore or set to zero the energy that turns evanescent. The proper thing to do with energy becoming evanescent at depth  $z$  is to save it for a second pass *upward*. The upward pass begins from the bottom of the section with a zero downgoing wave. As the downgoing wave is extrapolated upward, the saved evanescent energy is reintroduced. As usual, the images are

withdrawn from the wave at time  $t = 0$ .

To illustrate the concept, a program will be sketched that makes two images, first the usual image of the top side of the reflector, and second the image of the under side. The images may be viewed separately or summed.

The program makes the simplifying restriction on the velocity that  $dv/dz \geq 0$ . Because of this assumption, evanescent energy can be stored "in place" and ignored until the return pass. It is worth noting that the second pass is cheaper than the first pass because the region in which evanescence never occurred,  $|k| < |\omega|/v(\tau_{\max})$ , need not be processed.

```
# first pass of conventional phase-shift migration.
P(ω, kx) = FT[ u(t, x) ]
For τ = Δτ, 2Δτ, ..., τmax {
  For all kx {
    Uimage(kx, τ) = 0.
    For all ω > |k| v(τ) {
      C = exp(-i ω Δτ √(1 - v(τ)2 kx2/ω2))
      P(ω, kx) = P(ω, kx) * C
      Uimage(kx, τ) = Uimage(kx, τ) + P(ω, kx)
    }
  }
}
uimage(x, τ) = FT[Uimage(kx, τ)]
}
```

```
# Second pass for underside image.
For τ = τmax, τmax-Δτ, τmax-2Δτ, ..., 0 {
  For all kx {
    Dimage(kx, τ) = 0.
    For ω = |k| v(τ) to ω = |k| v(τmax) {
      # The wave changes direction but so does Δτ
      C = exp(-i ω Δτ √(1 - v(τ)2 kx2/ω2))
      P(ω, kx) = P(ω, kx) * C
      Dimage(kx, τ) = Dimage(kx, τ) + P(ω, kx)
    }
  }
}
dimage(x, τ) = FT[Dimage(kx, τ)]
}
```

### Stopping Phase-Shift Migration Wraparound (S. Levin)

Figure 1 shows a family of hyperbolas. Notice that these hyperbolas do not extend to infinite time but they truncate at a cut-off time  $t_c$ . A Fourier method will be described to create such time-truncated data. The method leads to a phase-shift migration program without wraparound artifacts.

When the fast Fourier transformation algorithm first came into use people noticed that it could be used for filtering. Transient filtering could be done exactly in the periodic Fourier domain if signals and filters were

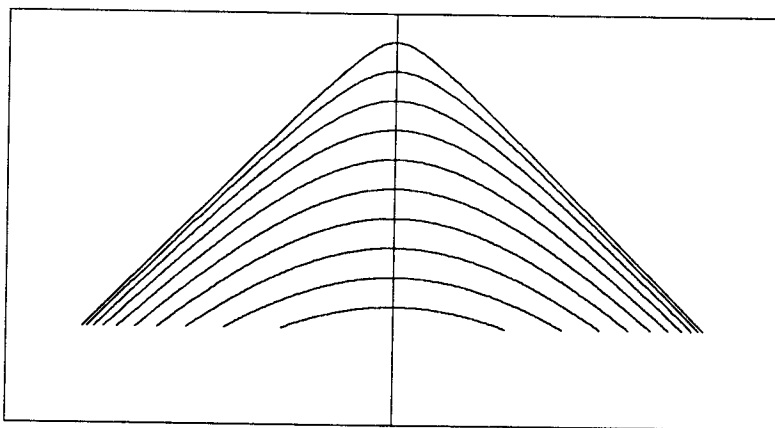


FIG. 4.5-1. Hyperbolas truncated at a particular time.

surrounded by enough zero padding. The same concept applies with migration. If field data and migration hyperbolas are surrounded by enough zeroes in the time- and space-domain then migration can be done in the Fourier domain with *no* wraparound. The trick is to see how the truncated hyperbolas in figure 1 can be constructed in the Fourier domain.

To have truncations at time  $t_c$ , special point sources must be used. The deeper the source, the narrower must be its angular aperture. Take a hyperbola with first arrival at time  $t_0$  to be truncated at some time  $t_c$ . The propagation angle  $\theta$  of energy at the cutoff is given by  $\cos \theta = t_0/t_c$ . So exploding reflectors have their  $k_x$ -spectrum truncated at  $\sin \theta = v k_x/\omega$ . A  $90^\circ$  aperture implies echoes with an infinite time delay. Here is a sketch of the program.

```

# Modeling with time truncation at  $t_c$ 
Model( $k_x, z$ ) = FT[ model( $x, z$ ) ]
For all  $\omega$  and all  $k_x$ 
    U( $\omega, k_x$ ) = 0.
For  $z = z_{\max}, z_{\max}-\Delta z, z_{\max}-2\Delta z, \dots, 0$  {
    For all  $\omega$  {
        For all  $|k_x| < |\omega|/v$  {
            if ( $z < v t_c$ ) {
                 $sine = \sqrt{1-z^2/v^2 t_c^2}$ 
                if(  $|v k_x| < |\omega| sine$  )
                     $aperture = 1.$ 
                else
                     $aperture = 0.$ 
            }
            else
                 $aperture = 0.$ 
        }
        U( $\omega, k_x$ ) = U( $\omega, k_x$ )  $e^{-i \Delta z \omega \sqrt{v^{-2} - k_x^2/\omega^2}}$  +  $aperture * Model(k_x, z)$ 
    }
}
}
u( $t, x$ ) = FT2D[ U( $\omega, k_x$ ) ]

```

The above modeling program may be converted to a migration program (as in Section 1.3) by running the depth  $z$  loop down instead of up and by multiplying the downward continued data by the aperture function. The modifications to the program not only improve the quality of the migration, but the calculation is faster.

### Controlling Stolt Migration Wraparound

As with the phase-shift algorithm, the key to reducing the computational artifacts of the Stolt algorithm is to suppress the time-domain wraparound. We will see that this amounts to accurate frequency-domain interpolation.

First, consider an impulse function at time  $t_0$ . Its Fourier transform is  $\exp(-i\omega t_0)$ . If  $t_0$  is large, then the Fourier transform is a rapidly oscillating function of  $\omega$ . Rapidly oscillatory functions are always difficult to interpolate. It is better to shift backward the time function, thereby smoothing its frequency function, then to interpolate the frequency function, and finally to undo the shift. Given seismic data on the time interval  $0 < t < T$ , the frequency function will be smoother if the data is shifted to an interval  $-T/2 < t < T/2$ . So the first proposed improvement to the Stolt migration program is to multiply in the frequency domain by  $\exp(i\omega T/2)$ , then interpolate, and finally multiply by  $\exp(-i\omega T/2)$ .

Linear interpolation is almost the easiest form of interpolation. On the other hand, Fourier transform theory suggests interpolation with the *sinc*

function (by definition  $\text{sinc } u = (\sin u)/u$ ). The *sinc* function of frequency, when brought back into the time domain is a rectangle function of time. Take this rectangle function to be nonzero on the interval  $-T/2 < t < T/2$ . Recall that the fast (inverse) Fourier transform algorithm sums at uniform intervals in the frequency domain. This implicitly assumes zero between sample points, which in turn assumes that the time-domain function is periodic outside the given time interval. Now take the rectangle function of time to be the multiplier in the time domain that converts the periodic time function to the observed transient one. This multiplication in the time domain is equivalent to a convolution in the frequency domain with the appropriate *sinc* function. Convolution of the continuous *sinc* function with the given discrete-interval frequency function is really interpolation. Unfortunately, the *sinc* function extends infinitely down the frequency axis. Worse yet, it decays slowly. So some approximation or truncation of the *sinc* is used. Bill Harlan showed that tapered *sinc* functions achieve satisfactory accuracy more cheaply than zero padding. It seems, however, that the best approach is both to zero pad and to use some *sinc*-like interpolation. A definitive study of interpolation is that of Rosenbaum and Boudreaux [1981].

### Stolt Stretch

The great strength and the great weakness of the Stolt migration method is that it uses Fourier transformation over depth. This is a strength because it makes his method much faster than all other methods. And it is a weakness because it requires a velocity that is a constant function of depth. The earth velocity typically ranges over a factor of two within the seismic section, and the effect of velocity on migration tends to go as its square. To ameliorate this difficulty, Stolt suggested stretching the time axis to make the data look more like it had come from a constant-velocity earth. Stolt proposed the stretching function

$$\tau(t) = \left[ \frac{2}{v_0^2} \int_0^t t v_{RMS}^2(t) dt \right]^{1/2} \quad (1a)$$

where

$$v_{RMS}^2(t) = \frac{1}{t} \int_0^t v^2(t) dt \quad (1b)$$

At late times, which are associated with high velocities, Stolt's stretch implies that  $\tau$  grows faster than  $t$ . The  $\tau$ -axis is uniformly sampled to allow the fast Fourier transform. Thus at late time the samples are increasingly dense

on the  $t$ -axis. This is the opposite of what earth  $Q$  and the sampling theorem suggest, but most people consider this a fair price.

The most straightforward derivation of (1) is based on the idea of matching the curvature of ideal hyperbola tops to the curvature on the stretched data. The equation of an ideal hyperbola in  $(x, \tau)$ -space is

$$v_0^2 \tau^2 = x^2 + z^2 \quad (2)$$

Simple differentiation shows that the curvature at the hyperbola top is

$$\left. \frac{d^2 \tau}{dx^2} \right|_{x=0} = \frac{1}{\tau v_0^2} \quad (3)$$

It can be shown that in a stratified medium, equation (3) applies, except that the velocity must be replaced by the RMS velocity:

$$\left. \frac{d^2 t}{dx^2} \right|_{x=0} = \frac{1}{t v_{RMS}^2} \quad (4)$$

We seek a stretched time  $\tau(t)$ . We would like to match the curves  $t(x)$  and  $\tau(x)$  for all  $x$ . But that would overdetermine the problem. Instead we could just match the derivatives at the hyperbola top, i.e., the second derivative of  $\tau[t(x)]$  with respect to  $x$  at  $x=0$ . With the substitutions (3) and (4), this would give an expression for  $\tau d\tau/dt$  which, after integrating and taking its square root, yields (1).

A different derivation of the stretch gives a more accurate result at steeper angles. Instead of matching hyperbola curvature at the top, we go some distance out on the flank and match the slope and value. It is the flanks of the hyperbola that actually migrate, not the tops, so this result is more accurate. Algebraically the derivation is also easier, because only *first* derivatives are needed. Differentiating equation (2) with respect to  $x$  for a reflector at any depth  $z_j$  gives

$$\frac{d\tau}{dx} = \frac{x}{\tau v_0^2} \quad (5)$$

There is an analogous expression in a stratified medium. To obtain it, solve  $x = \int v \sin \theta dt = p \int v^2 dt$  for  $p = dt/dx$ :

$$\frac{dt}{dx} = \frac{x}{\int_0^t v^2(p, t) dt} \quad (6)$$

Expressions (5) and (6) play the same role as (3) and (4), but (5) and (6) are valid everywhere, not just at the hyperbola top. Differentiating  $\tau(t)$  gives



$$\frac{d\tau}{dx} = \frac{d\tau}{dt} \frac{dt}{dx} \quad (7)$$

Inserting (5) and (6) into (7) gives

$$\frac{x}{\tau v_0^2} = \frac{d\tau}{dt} \frac{x}{\int_0^t v^2(p, t) dt} \quad (8)$$

$$\tau d\tau = \left[ \frac{1}{v_0^2} \int_0^t v^2(p, t') dt' \right] dt \quad (9)$$

Integrating (9) gives  $\tau^2/2$  on the left. Then, taking the square root gives (1a) but with a new definition for RMS velocity:

$$v_{RMS}^2(t) = \frac{1}{t} \int_0^t v^2(p, t) dt \quad (1c)$$

The thing that is new is the presence of the Snell parameter  $p$ . In a stratified medium characterized by some velocity, say,  $v'(z)$ , the velocity  $v(p, t)$  is defined for the tip of the ray that left the surface at an angle with a stepout  $p$ . In practice, what value of  $p$  should be used? The best procedure is to look at the data and measure the  $p = dt/dx$  of those events that you wish to migrate well. A default value is  $p = 2(\sin 30^\circ)/(2.5 \text{ km/sec}) = .4 \text{ millsec/meter}$ . The factor of 2 is from the exploding-reflector model.

### Gazdag's $v(x)$ Method

The phase-shift method of migration is attractive because it allows for arbitrary depth variation in velocity and arbitrary angles of propagation up to  $90^\circ$ . Unfortunately, lateral variation in velocity is not permitted because of the Fourier transformation over the  $x$ -axis. To alleviate this difficulty, Gazdag and Sguazzero [1984] proposed an interpolation method. Recall from Section 1.3 that the phase-shift method 2-D Fourier transforms the data  $p(x, t)$  to  $P(k_x, \omega)$ . Then  $P(k_x, \omega)$  is downward continued in steps of depth by multiplication with  $\exp[ik_z(\omega, k_x) \Delta z]$ . Gazdag proposed several reference velocities, say,  $v_1, v_2, v_3$ , and  $v_4$ . He downward continued one depth step with each of the velocities, obtaining several reference copies of the downward-continued data, say,  $P_1, P_2, P_3$ , and  $P_4$ . Then he inverse Fourier transformed each of the  $P_j$  over  $k_x$  to  $p_j(x, \omega)$ . At each  $x$ , he interpolated the reference waves of nearest velocity to get a final value, say,  $p(x, \omega)$

which he retransformed to  $P(k_x, \omega)$  ready for another step. This appears to be an inefficient method since it duplicates the usual migration computation for each velocity. Surprisingly, the method seems to be successful, perhaps because of the peculiar nature of computation using an array processor.

### EXERCISE

1. To obtain a sharp cutoff in time  $t_c$  requires a broad bandwidth in the spectral domain. Given that figure 1 is expressed on a  $1000 \times 1000$  mesh, deduce the uncertainty in the cutoff  $t_c$ .
2. The phase-shift method tends to produce a migration that is periodic with  $z$  because of the periodicity of the Fourier transform over  $t$ . Ordinarily, this is not troublesome because we do not look at large  $z$ . The upcoming wave at great depth should be zero *before*  $t=0$ . Kjartansson pointed out that periodicity in  $z$  could be avoided if the wave at  $t=0$  is subtracted from the wavefield before the computation descends further. Thus, information could never get to negative time and “wrap around.” Indicate how the program should be changed.

## 4.6 Impedance

Classical physics gives much attention to energy conservation and dissipation. Engineering filter theory gives much attention to causality — that there can be no response before the excitation. In geophysics we often need to ensure both causality and energy loss. We need to incorporate both, not only in theoretical derivations, but also in computations, and sometimes in computations that are discretized in time. There is a special class of mathematical functions called *impedance* functions that describe causal, linear disturbances in physical objects that dissipate energy.

Nature evolves forward in time. Naturally, impedance functions play a fundamental role in any modeling calculation where time evolves from past to future. Besides their use in physical modeling, impedances also find use in the depth extrapolation of waves. We geophysicists take data on the earth's

surface and extrapolate downward to get information at depth. It is not the same as nature's extrapolation in time. In principle we don't require impedance functions to extrapolate in depth. But depth extrapolations made without impedance functions could exhibit growing oscillations, much like a physical system receiving energy from an external source. In fact, "straight-forward" implementations of physical equations often exhibit unstable extrapolations. By formulating our extrapolation problems with impedance functions, we ensure stability. Of all the virtues a computational algorithm can have — stability, accuracy, clarity, generality, speed, modularity, etc. — the most important seems to be stability.

In this section we examine the theory of impedance functions, their precise definition, their computation in the world of discretized time, and the rules for combining simple impedances to get more complicated ones. We will also examine other special functions, the *minimum-phase* filter and the *reflectance* filter in their relation to the impedance filter. Wide-angle wave extrapolation and migration in the time domain will be formulated with impedance functions. Rocks are unlike "pure" substances because they contain irregularities at all scales. A particularly simple impedance function will be found that mimics the dissipation of energy in rocks, unlike the classical equations of Newtonian viscoelasticity.

### **Beware of Infinity!**

To prove that one equals zero take an infinite series, for example, 1, -1, +1, -1, +1,  $\dots$  and group the terms in two different ways, and add them in this way:

$$\begin{aligned} (1-1) + (1-1) + (1-1) + \dots &= 1 + (-1+1) + (-1+1) + \dots \\ 0 + 0 + 0 + \dots &= 1 + 0 + 0 + \dots \\ 0 &= 1 \end{aligned}$$

Of course this does not prove that one equals zero: it proves that care must be taken with infinite series. Next, take another infinite series in which the terms may be regrouped into any order without fear of paradoxical results. Let a pie be divided into halves. Let one of the halves be divided in two, giving two quarters. Then let one of the two quarters be divided into two eighths. Continue likewise. The infinite series is  $1/2, 1/4, 1/8, 1/16, \dots$ . No matter how the pieces are rearranged, they should all fit back into the pie plate and exactly fill it.

The danger of infinite series is not that they have an infinite number of terms but that they may sum to infinity. Safety is assured if the sum of the absolute values of the terms is finite. Such a series is called *absolutely convergent*.

### Z - transform

The  $Z$ -transform of an arbitrary, time-discretized function  $x_t$  is defined by

$$X(Z) = \cdots x_{-2} Z^{-2} + x_{-1} Z^{-1} + x_0 + x_1 Z + x_2 Z^2 + \cdots \quad (1)$$

Give  $Z$  the physical interpretation of time delay by one time unit. Then  $Z^2$  delays two time units. Expressions like  $X(Z)U(Z)$  and  $X(Z)U(1/Z)$  are useful because they imply convolution and cross-correlation of the time-domain coefficients. (See FGDP).

Going on to consider numerical values for the delay operator  $Z$ , we discover that it is useful to ask whether  $X(Z)$  is finite or infinite. Numerical values of  $Z$  that are of particular interest are  $Z=+1$ ,  $Z=-1$ , and all those complex values of  $Z$  which are unit magnitude, say,  $|Z|=1$  or

$$Z = e^{i\omega\Delta t} \quad (2)$$

where  $\omega$  is the real Fourier transform variable. Taking  $\omega$  to be real means that  $Z$  is on the unit circle. Then the  $Z$ -transform is a discrete Fourier transform. Our attention can be restricted to time functions with a finite amount of energy by demanding that  $U(Z)$  be finite for all values of  $Z$  on the unit circle  $|Z|=1$ . Filter functions are always restricted to have finite energy.

The most straightforward way to say that a filter is causal is to say that its time domain coefficients vanish before zero lag, that is  $u_t=0$  for  $t<0$ . Another way to say it is to say that  $U(Z)$  is finite for  $Z=0$ . At  $Z=0$  the  $Z$ -transform would be infinite if the coefficients  $u_{-1}$ ,  $u_{-2}$ , etc. were not zero. For a causal function, each term in  $|U(Z)|$  will be smaller if  $Z$  is taken inside the disk  $|Z|<1$  rather than on it. Thus convergence at  $Z=0$  and on the circle  $|Z|=1$  implies convergence everywhere inside the unit disk. So boundedness combined with causality means convergence in the unit disk. Convergence at  $Z=0$  but not on the circle  $|Z|=1$  would refer to a causal function with infinite energy, a case of no practical interest. What kind of function converges on the circle, at  $Z=\infty$ , but not at  $Z=0$ ? What function converges at all three places,  $Z=0$ ,  $Z=\infty$ , and  $|Z|=1$ ?

The filter  $1/(1 - 2Z)$  can be expanded into powers of  $Z$  in (at least) two different ways. These are

$$\begin{aligned} \frac{1}{1 - 2Z} &= 1 + 2Z + 4Z^2 + 8Z^3 + \dots \\ &= -\frac{1}{2Z} \frac{1}{1 - \frac{1}{2Z}} = -\frac{1}{2Z} \left[ 1 + \frac{1}{2Z} + \frac{1}{4Z^2} + \dots \right] \end{aligned} \quad (3)$$

Which of these two infinite series converges depends on the numerical value of  $Z$ . For  $|Z| = 1$  the first series diverges, but the second converges. So the only acceptable filter is *anticausal*. Is a series expansion unique? It is if it converges. Complex-variable theory proves this.

Let  $b_t$  denote a filter. Then  $a_t$  is its inverse filter if the convolution of  $a_t$  with  $b_t$  is a delta function. In the Fourier domain, we would say that filters are inverse to one another if their Fourier transforms are inverse to one another.  $Z$ -transforms can be used to define the inverse filter, say,  $A(Z) = 1/B(Z)$ . Whether the filter  $A(Z)$  is causal depends on whether it is finite everywhere inside the unit disk, or really on whether  $B(Z)$  vanishes *anywhere* inside the disk. For example,  $B(Z) = 1 - 2Z$  vanishes at  $Z = 1/2$ . There  $A(Z) = 1/B(Z)$  must be infinite, that is to say, the series  $A(Z)$  must be nonconvergent at  $Z = 1/2$ . Thus — as we have just seen —  $a_t$  is noncausal. A most interesting case, called *minimum phase*, occurs when both a filter  $B(Z)$  and its inverse are causal. In summary:

<i>causal</i>	$ B(Z)  < \infty$ for $ Z  \leq 1$
<i>causal inverse</i>	$ 1/B(Z)  < \infty$ for $ Z  \leq 1$
<i>minimum phase</i>	<i>both above conditions</i>

### Review of Impedance Filters

Use  $Z$ -transform notation to define a filter  $R(Z)$ , its input  $X(Z)$ , and its output  $Y(Z)$ . Then

$$Y(Z) = R(Z) X(Z) \quad (4)$$

The filter  $R(Z)$  is said to be *causal* if the series representation of  $R(Z)$  has no negative powers of  $Z$ . In other words,  $y_t$  is determined from present and past values of  $x_t$ . Additionally, the filter  $R(Z)$  is *minimum*

phase if  $1/R(Z)$  has no negative powers of  $Z$ . This means that  $x_t$  can be determined from present and past values of  $y_t$  by straightforward polynomial division in

$$X(Z) = \frac{Y(Z)}{R(Z)} \quad (5)$$

Given that  $R(Z)$  is already minimum phase, it can in addition be an impedance function if positive energy or work is represented by

$$0 \leq \text{work} = \sum_t \text{force} \times \text{velocity} = \sum_t \text{voltage} \times \text{current} \quad (6a)$$

$$= \frac{1}{2} \sum_t (\bar{x}_t y_t + \bar{y}_t x_t) \quad (6b)$$

$$= \text{coef of } Z^0 \text{ of } \left[ \bar{X} \left[ \frac{1}{Z} \right] Y(Z) + \bar{Y} \left[ \frac{1}{Z} \right] X(Z) \right] \quad (6c)$$

$$= \frac{1}{2\pi} \int_0^{2\pi} \text{Re} (\bar{X} Y) d\omega \quad (6d)$$

$$= \int \text{Re} (\bar{X} R X) d\omega = \int \bar{X} X \text{Re} (R) d\omega \quad (6e)$$

Since  $\bar{X}X$  could be an impulse function located at any  $\omega$ , it follows that  $\text{Re} [R(\omega)] \geq 0$  for all real  $\omega$ . In summary:

<i>Definition of an Impedance</i>	
<i>causality</i>	$r_t = 0$ for $t < 0$ i.e. $ R(Z)  < \infty$ for $ Z  \leq 1$
<i>causal inverse</i>	$ 1/R(Z)  < \infty$ for $ Z  \leq 1$
<i>dissipates energy</i>	$2 \text{Re} R(\omega) = R(Z) + \bar{R}(1/Z) \geq 0$ real $\omega$

Adding an impedance to its Fourier conjugate gives a real positive function (the imaginary part of which is zero) like a power spectrum, say,

$$\left( r_0 + r_1 Z + r_2 Z^2 + \dots \right) + \quad (7a)$$

$$\left( \bar{r}_0 + \bar{r}_1 \frac{1}{Z} + \bar{r}_2 \frac{1}{Z^2} + \dots \right) \geq 0 \text{ for real } \omega$$

$$R(Z) + \bar{R} \left[ \frac{1}{Z} \right] \geq 0 \text{ for real } \omega \quad (7b)$$

which is the basis for the remarkable fact that every impedance time function is one side of an autocorrelation function.

Impedances also arise in economic theory when  $X$  and  $Y$  are price and sales volume. I suppose that there the positivity of the impedance means that in the game of buying and selling you are bound to lose!

### Causal Integration

Begin with a function in discretized time  $p_t$ . The Fourier transform with the substitution  $Z = \exp(i\omega \Delta t)$  is the  $Z$ -transform

$$P(Z) = \cdots p_{-2} Z^{-2} + p_{-1} Z^{-1} + p_0 + p_1 Z + p_2 Z^2 + \cdots \quad (8)$$

Define  $-i\hat{\omega}$  (which will turn out to be an approximation to  $-i\omega$ ) by

$$\frac{1}{-i\hat{\omega} \Delta t} = \frac{1}{2} \frac{1+Z}{1-Z} \quad (9)$$

Define another time function  $q_t$  with  $Z$ -transform  $Q(Z)$  by applying the operator to  $P(Z)$ :

$$Q(Z) = \frac{1}{2} \frac{1+Z}{1-Z} P(Z) \quad (10)$$

Multiply both sides by  $(1-Z)$ :

$$(1-Z) Q(Z) = \frac{1}{2} (1+Z) P(Z) \quad (11)$$

Equate the coefficient of  $Z^t$  on each side:

$$q_t - q_{t-1} = \frac{p_t + p_{t-1}}{2} \quad (12)$$

Taking  $p_t$  to be an impulse function, we see that  $q_t$  turns out to be a step function, that is,

$$p = \cdots 0, 0, 0, 0, 0, 1, 0, 0, 0, 0, 0, 0, \cdots \quad (13a)$$

$$q = \cdots 0, 0, 0, 0, 0, \frac{1}{2}, 1, 1, 1, 1, 1, 1, \cdots \quad (13b)$$

So  $q_t$  is the discrete domain representation of the integral of  $p_t$  from minus infinity to time  $t$ . It is the same as a Crank-Nicolson-style numerical integration of the differential equation  $dQ/dt = P$ . The operator  $(1+Z)/(1-Z)$  is called the bilinear transform. The accuracy of the approximation to differentiation can be seen by multiplication on top and bottom by  $Z^{-.5}$  and substitution of  $Z = e^{i\omega\Delta t}$ .

$$-i \frac{\hat{\omega} \Delta t}{2} = \frac{1-Z}{1+Z} = \frac{Z^{-.5} - Z^{+.5}}{Z^{-.5} + Z^{+.5}} = \quad (14a)$$

$$-i \frac{\hat{\omega} \Delta t}{2} = -i \frac{\sin \omega \Delta t / 2}{\cos \omega \Delta t / 2} = -i \tan \frac{\omega \Delta t}{2} \quad (14b)$$

The integration operator has a pole at  $Z=1$ , which is exactly on the unit circle. This raises the possibility of the paradox of infinity. In other words, there are other noncausal expansions too. For example, taking  $1/(-i\omega)$  to be an imaginary, antisymmetric function of  $\omega$  implies a real, antisymmetric time function, namely,  $\text{sgn}(t) = t/|t|$ , which is not usually regarded as the integration operator. To avoid any ambiguity, we introduce here a small positive number  $\epsilon$  and define  $\rho = 1 - \epsilon$ . The integration operator becomes

$$I = \frac{1}{2} \frac{1 + \rho Z}{1 - \rho Z} \quad (15a)$$

$$= \frac{1}{2} (1 + \rho Z) \left[ 1 + \rho Z + (\rho Z)^2 + (\rho Z)^3 + \dots \right] \quad (15b)$$

$$= \frac{1}{2} + \rho Z + (\rho Z)^2 + (\rho Z)^3 + \dots \quad (15c)$$

Because  $\rho$  is slightly less than one, this series converges for any value of  $Z$  on the unit circle. If  $\epsilon$  had been slightly negative instead of positive the expansion would have come out in negative instead of positive powers of  $Z$ .

Now the big news is that the causal integration operator is an example of an impedance function. The operator is clearly causal with a causal inverse. Let us check in the frequency domain that the real part is positive. Rationalizing the denominator gives

$$I = \frac{1}{2} \frac{(1 + \rho Z)}{(1 - \rho Z)} \frac{(1 - \rho/Z)}{(1 - \rho/Z)} = \frac{(1 - \rho^2) + \rho(Z - 1/Z)}{\text{positive}} \quad (16a)$$

$$= \frac{(1 - \rho^2) + 2i\rho \sin \omega \Delta t}{\text{positive}} \quad (16b)$$

Again, it is the choice of a positive  $\epsilon$  that has caused  $1 - \rho^2$ , and hence the real part to be positive for all  $\omega$ , as shown in figure 1.

As multiplication by  $-i\omega$  in the frequency domain is associated with differentiation  $d/dt$  in the time domain, so is division by  $-i\omega$  associated with integration. People usually associate the asymmetric operator  $(1, -1)$  with differentiation. But notice that the inverse to the causal integration operator, namely,

$$I^{-1} = 2 \frac{1 - \rho Z}{1 + \rho Z} \quad (17a)$$



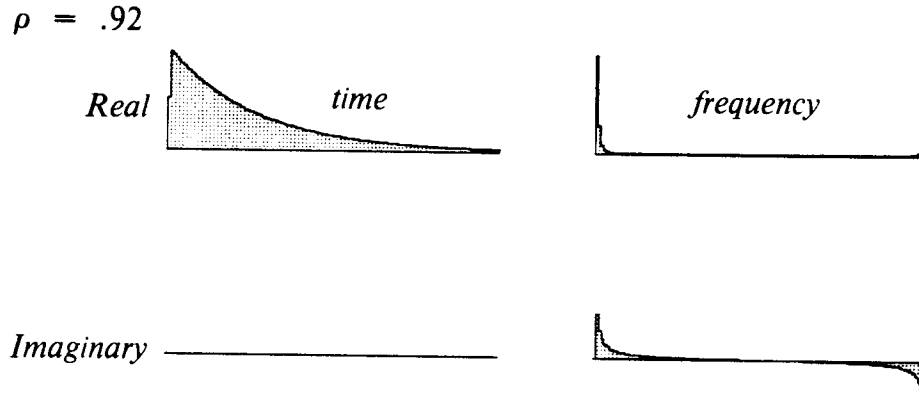


FIG. 4.6-1. The causal integration operator  $I$ . The frequency axis is represented by a discrete Fourier transform over 256 points. Zero time and zero frequency are on the left end of their respective axes.

$$I^{-1} = 2 - 4\rho Z + 4(\rho Z)^2 - 4(\rho Z)^3 + \dots \quad (17b)$$

also represents differentiation, although it is completely causal and not at all asymmetric. In linear systems analysis this representation of discrete differentiation is often the preferred one. The construction of higher-order, stable differential equations is subject to certain rules, to be covered, for combining impedances.

Occasionally it is necessary to have a *negative* real part for the differentiation operator. This can be achieved by taking  $\epsilon$  to be negative, which means taking  $\rho > 1$ , and doing the infinite series expansion in powers of  $Z^{-1}$ , that is, anticausally instead of causally. In either the anticausal or the causal case the imaginary part will still be  $-i\omega$ , but the real part will have the opposite sign.

### Muir's Rules for Combining Impedances

For every physical system that conserves or dissipates energy there is an impedance function. Impedance functions are *special* combinations of differential operators and positive-valued physical constants. We will see just what combinations are allowed.

To ensure stable computations, it is important to be able to ensure that a supposed impedance function really is an impedance function. A difficulty in applied geophysics is this: Although you might require results only over a limited range of frequencies, and you might make approximations that are

reasonable within that range, if the calculated impedance becomes negative outside the applicable range (it often happens near the Nyquist frequency), then the impedance filter will yield a numerically divergent output. So even though the impedance is almost correct, it is not usable.

Francis Muir provided† three rules for combining simple impedances to get more complicated ones. These rules are especially useful because we can start from the discrete-time forms of the differentiation and integration operators. Let  $R'$  denote a new impedance function generated from known impedance functions  $R$ ,  $R_1$ , and  $R_2$ . These three ways of combining impedance are

- |  |                    |
|--|--------------------|
| 1. Multiplication by positive scalar $a$ | $R' = a R$         |
| 2. Inversion                             | $R' = \frac{1}{R}$ |
| 3. Addition                              | $R' = R_1 + R_2$   |

These rules do not include multiplication. Multiplication is not allowed because squaring, for example, doubles the phase angle, and thus may destroy the positivity of the real part. Since these rules do not include multiplication, but only scaling, summation, and inversion, the impedance functions that occur in nature will often be represented mathematically as *continued fractions*.

The first two of Muir's rules are so obvious we will not prove them. The third rule deserves more careful attention. To prove any rule, we need to show three things about  $R'$ , namely, it is causal, it is PR (the Fourier transform has a positive real part), and it has an inverse. This last part is the hard part with Muir's third rule, namely, that the sum of two impedances has a causal inverse. Proof of this fact will take about two pages, and introduce several additional concepts.

### Impedance Defined from Reflectance

The size of the class of filters called *impedances* will be seen to be large, because impedances are derived by transformation from an easily specified family of filters called *reflectances*, say,  $c_t$  and its Fourier transform  $C(\omega)$ . To be a reflectance, the time function must be strictly causal, and the frequency function must be strictly less than unity. By *strictly causal* it is meant that the time function vanishes both at zero time and before. For example, take  $-1 < \rho < +1$  and the reflectance  $c_t$  to be an impulse of size

†Personal communication with Francis Muir.

$\rho$  after a time  $\Delta t$ . The Fourier transform is

$$C = \rho Z = \rho e^{i\omega\Delta t} \quad (18)$$

Obviously, the product of two reflectances is another reflectance.

An impedance has been defined to be a causal filter with a causal inverse and a Fourier transform whose real part is positive. It will be shown that from any reflectance  $C$  the expression

$$R = \frac{1 - C}{1 + C} \quad (19)$$

generates an impedance. There are three things to show:  $R$  is causal, has a causal inverse, and is PR. First because of the assumption that  $C$  has a magnitude strictly less than unity,  $C \bar{C} < 1$ , the denominator expands to a convergent  $1 + C + C^2 + \dots$ . Second, the inverse of  $R$  is found by simply changing the sign of  $C$ . Third, multiply top and bottom by the complex conjugate:

$$\operatorname{Re} R = \operatorname{Re} \frac{(1 - C)(1 + \bar{C})}{\text{positive}} \stackrel{?}{\geq} 0 \quad (20a)$$

$$\operatorname{Re} R = \operatorname{Re} \frac{(1 - C \bar{C}) + \text{imaginary}}{\text{positive}} \geq 0 \quad (20b)$$

which shows that  $R$  has a real part that is positive.

The expression for  $R(C)$  is easily back-solved for  $C(R)$ , but the converse theorem, that every  $R$  generates a reflectance, is harder to show. Nevertheless, it will be proved, along with a deeper theorem. A filter that is both causal and PR is said to be CPR. The deeper theorem is that *every CPR has an inverse and hence is an impedance*. This will be proved by showing that every CPR — say,  $\hat{R}$ , — can be used to construct a reflectance  $\hat{C}$ , which, since it is a reflectance, implies that the CPR  $\hat{R}$  is an impedance  $R$ . Backsolving gives

$$\hat{C} = \frac{1 - \hat{R}}{1 + \hat{R}} \quad (21)$$

Proof requires that two things be shown — first, that the magnitude of  $\hat{C}$  is less than unity. To show this, form the magnitude of the denominator and subtract the magnitude of the numerator. The result is four times the real part of  $\hat{R}$ , which is positive. Second,  $\hat{C}$  must be proved causal. This is harder.  $(1 + \hat{R})^{-1}$  can be expanded into a sum of positive powers of  $\hat{R}$  and hence of positive powers of the delay operator. But the convergence of the series is not assured, because nothing requires  $\hat{R}$  to be less than unity.

assure us that (24) always converges, so  $b_t$  is always causal.

To establish theorem 2, that the exponential is not just causal but also minimum phase, consider

$$B_+ = e^{+U} \quad (25a)$$

$$B_- = e^{-U} \quad (25b)$$

Clearly both  $B_+$  and  $B_-$  are causal, and they are inverses of one another. A minimum-phase filter is defined to be causal with a causal inverse. So  $B_+$  and  $B_-$  are minimum phase.

Now we will establish the converse of theorem 2 — namely, theorem 3 — which states that the logarithm of a minimum-phase filter is causal. Take the logarithm of (24) and form the  $Z$ -derivative:

$$U = \ln B \quad (26a)$$

$$\frac{dU}{dZ} = u_1 + 2u_2Z + 3u_3Z^2 + \dots \quad (26b)$$

$$\frac{dU}{dZ} = \frac{1}{B} \frac{dB}{dZ} \quad (26c)$$

Since  $B$  was assumed to be minimum phase, both  $1/B$  and  $dB/dZ$  on the right of (26c) are causal. Since the product of two causals is causal,  $dU/dZ$  is causal. But  $dU/dZ$  cannot be causal unless  $U$  is causal. That proves theorem 3, disregarding the remote danger that  $B$  might converge while  $dB/dZ$  diverges.

Theorem 4 refers to the Fourier domain representation of the minimum-phase filter. In the complex plane, the filter gives parametric equations for a curve, say  $[x(\omega), y(\omega)] = [\text{Re } B(Z), \text{Im } B(Z)]$ . The phase angle  $\phi(\omega)$  is defined by the arctangent of the ratio  $y/x$ . For example, the causal, non-minimum-phase filter  $U(Z) = Z = e^{i\omega}$  gives the parametric equations  $x = \cos \omega$  and  $y = \sin \omega$  which define a circle surrounding the origin. Notice that the phase of  $Z = e^{i\omega}$  is  $\phi(\omega) = \omega$ , which is a monotonically increasing function of  $\omega$ . In the minimum phase case,  $\phi(\omega=0) = \phi(\omega=2\pi)$ . In the non-minimum-phase case, the curve loops the origin, so  $\phi(\omega=0) = \phi(\omega=2\pi) + 2\pi$ . Theorem 3 allows us to say that a general formula for minimum-phase filters is

$$B = e^{U(Z)} = \exp \left\{ \sum_{k=0}^N U_k \cos k\omega + i \sum_{k=0}^N U_k \sin k\omega \right\} \quad (27a)$$

$$= \exp[r(\omega) + i \phi(\omega)] \quad (27b)$$

The phase  $\phi(\omega)$ , being a sum of periodic functions, is itself a periodic function of  $\omega$ , which means that in the plane of  $(\text{Re } B, \text{Im } B)$  the curve representing  $B(\omega)$  does not enclose the origin.

On to theorem 5, which says that any power of a minimum-phase function is minimum phase. Consider

$$B^r = (e^{\ln B})^r = e^{r \ln B} \quad (28)$$

Since  $B$  is assumed to be minimum phase, by theorem 3  $\ln B$  will be causal. Scaling by a real or complex constant  $r$  does not change causality. Exponentiating shows, by theorem 2, that  $B^r$  is minimum phase.

Finally the proof of theorem 6, that an impedance function can be raised to any real fractional power  $-1 \leq \rho \leq +1$  and the result will still be an impedance function. An impedance function is defined to be a minimum-phase function with the additional property that the real part of its Fourier transform is positive. This means that the phase angle  $\phi$  lies in the range  $-\pi/2 < \phi < +\pi/2$ . Raising the impedance function to the  $\rho$  power will compress the range to  $-\pi\rho/2 < \phi < \pi\rho/2$ . This will keep the real part of the impedance function positive. Theorem 5 states that any power of a minimum-phase function is causal, which is more than we need to be certain that a *fractional* real power of an impedance function will be causal.

### Wide-Angle Wave Extrapolation

Let  $s = -i \hat{\omega}$  denote the causal, positive, discrete representation of the differentiation operator, say,

$$s = -i \hat{\omega} = \frac{2}{\Delta t} \frac{1 - \rho Z}{1 + \rho Z} \quad (29)$$

Figure 2 compares hyperbolas constructed with  $\omega$  to those constructed with  $\hat{\omega}$ . You see a pleasing drop in wraparound noise. It seems to work better than the  $\epsilon$  in Section 4.1. As we will see, the introduction of complex-valued  $\hat{\omega}$  leads to a more natural handling of the square root at the evanescent transition.

Consider the following recursion starting from  $R_0 = s$ :

$$R_{n+1} = s + \frac{X^2}{s + R_n} \quad (30)$$

This recursion produces continued fractions. Francis Muir introduced it as a means of developing wide-angle square-root approximations for migration (Section 2.1), and he developed his three rules to show that every  $R_n$  is an impedance function. To see why every  $R_n$  is an impedance function, first

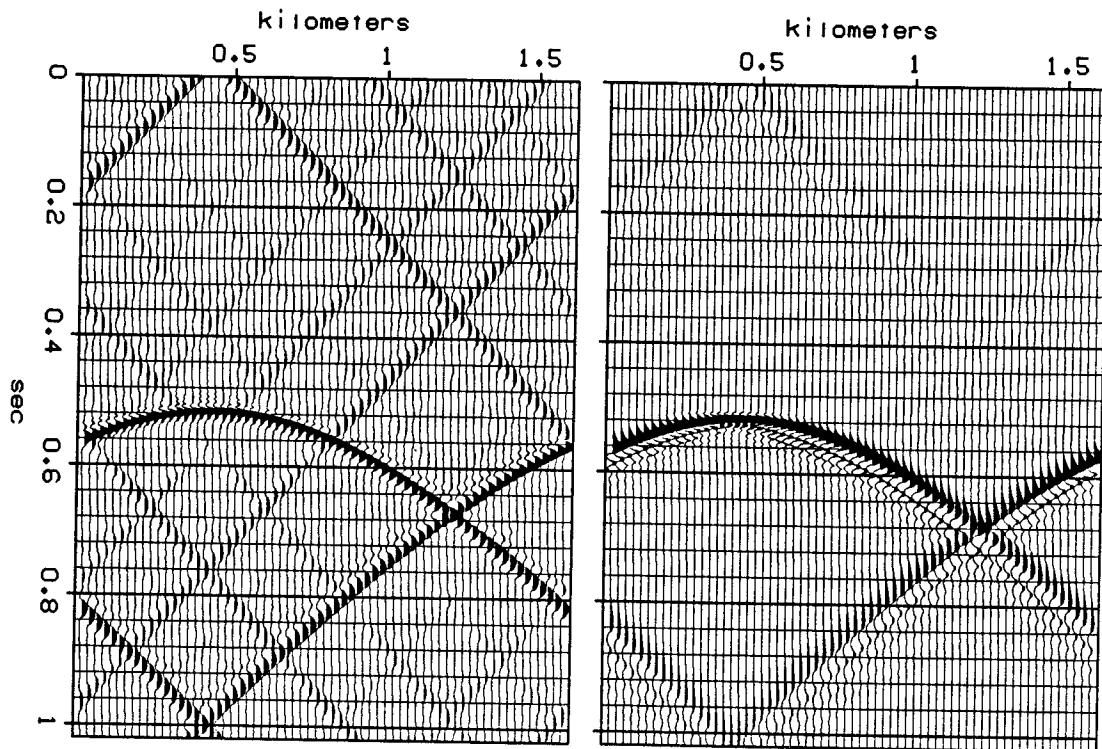


FIG. 4.6-2. Hyperbolas with real frequency (left) and complex frequency (right). (Plotting uses square root gain described in Section 4.1).

note that the denominator  $s + R_n$  is, for  $n = 0$ , the sum of two impedance functions. Then its inverse is an impedance function, and multiplication by the real positive constant  $X^2$  and addition of another  $s$  both preserve the properties of impedance functions. Recursively we see that all the  $R_n$  are impedances.

As  $N$  becomes large this recursion either converges or it does not. Supposing that it does, we can see what it will converge to by setting  $R_{n+1} = R_n = R_\infty = R$ . Thus,

$$R = s + \frac{X^2}{s + R} \quad (31a)$$

$$R(s + R) = s(s + R) + X^2 \quad (31b)$$

$$R^2 = s^2 + X^2 \quad (31c)$$

$$R = \sqrt{s^2 + X^2} \quad (31d)$$

In wave-extrapolation problems  $X^2$  is  $v^2 k_x^2$ , where  $v$  is the wave velocity and  $k_x$  is the horizontal spatial frequency, namely, the Fourier dual to the horizontal  $x$ -axis. Performing these substitutions we have

$$R = \pm \sqrt{-\hat{\omega}^2 + v^2 k_x^2} \quad (32)$$

So  $R$  is like  $\pm i k_z v$ . Remember that  $R_0$ , the first approximation to  $R$ , is  $-i\hat{\omega}$ . So downgoing waves are

$$D(x, z, t) = D(x, 0, t) e^{i k_x x} e^{-R z/v} e^{-i\omega t} \quad (33)$$

To switch from downgoing to upcoming waves, we could either change the sign in front of  $R$  or we take the complex conjugate of  $R$ . The difference is what you want to do with the real part — do you want the wave to grow or not?

Consider the dissipation of waves in the exploding reflector model. They damp as they propagate from the explosion to the surface. This means that as we migrate them, they should be exponentially growing. But we don't really want that. We really want to assure that they are not growing, perhaps we even want them decaying as we extrapolate them back. So for migration we downward continue monochromatic waves with

$$U(x, z, t) = U(x, 0, t) e^{i k_x x} e^{-\bar{R} z/v} e^{-i\omega t} \quad (34)$$

although the real behavior of a wave from an exploding reflector wave would be

$$U(x, z, t) = U(x, 0, t) e^{i k_x x} e^{+R z/v} e^{-i\omega t} \quad (35)$$

To examine the phase of the complex quantity  $R$ , set  $v = 1$  obtaining

$$R = \sqrt{(-i\hat{\omega})^2 + k_x^2} \quad (36)$$

First note that  $(-i\hat{\omega})$  is causal because of its  $Z$ -transform representation. By squaring the  $Z$ -transform we see that  $(-i\hat{\omega})^2$  is also causal. In the time domain,  $k_x^2$  is a delta function at the time origin. Thus  $R^2$  given by (36) is causal. Figure 3 shows how the phase of (36) is constructed from its constituents. To illustrate the behavior of  $-i\hat{\omega}$  from zero to infinity, I include both an artist's conception and the function on itself, overlain at various magnifications. The function  $-i\hat{\omega}$  is a periodic with  $\omega$  and its real and imaginary parts plot to a closed curve. To show the rate of change of the function, I sampled  $\omega$  at  $2^\circ$  intervals. From great distance the function is a circle. Close up it looks like a line parallel to the imaginary axis.

$R^2$  is causal and from figure 3 we can see that it has a "branch cut" property. That is, the phase of  $R$  has the positive real property. Theorem 5 forces  $R$  to be causal and minimum phase. That, with the phase defined by figure 3, proves that  $R$ , given by (36), is an impedance function.

$$-i\hat{\omega} = 2 \frac{1 - .9 e^{i\omega}}{1 + .9 e^{i\omega}}$$

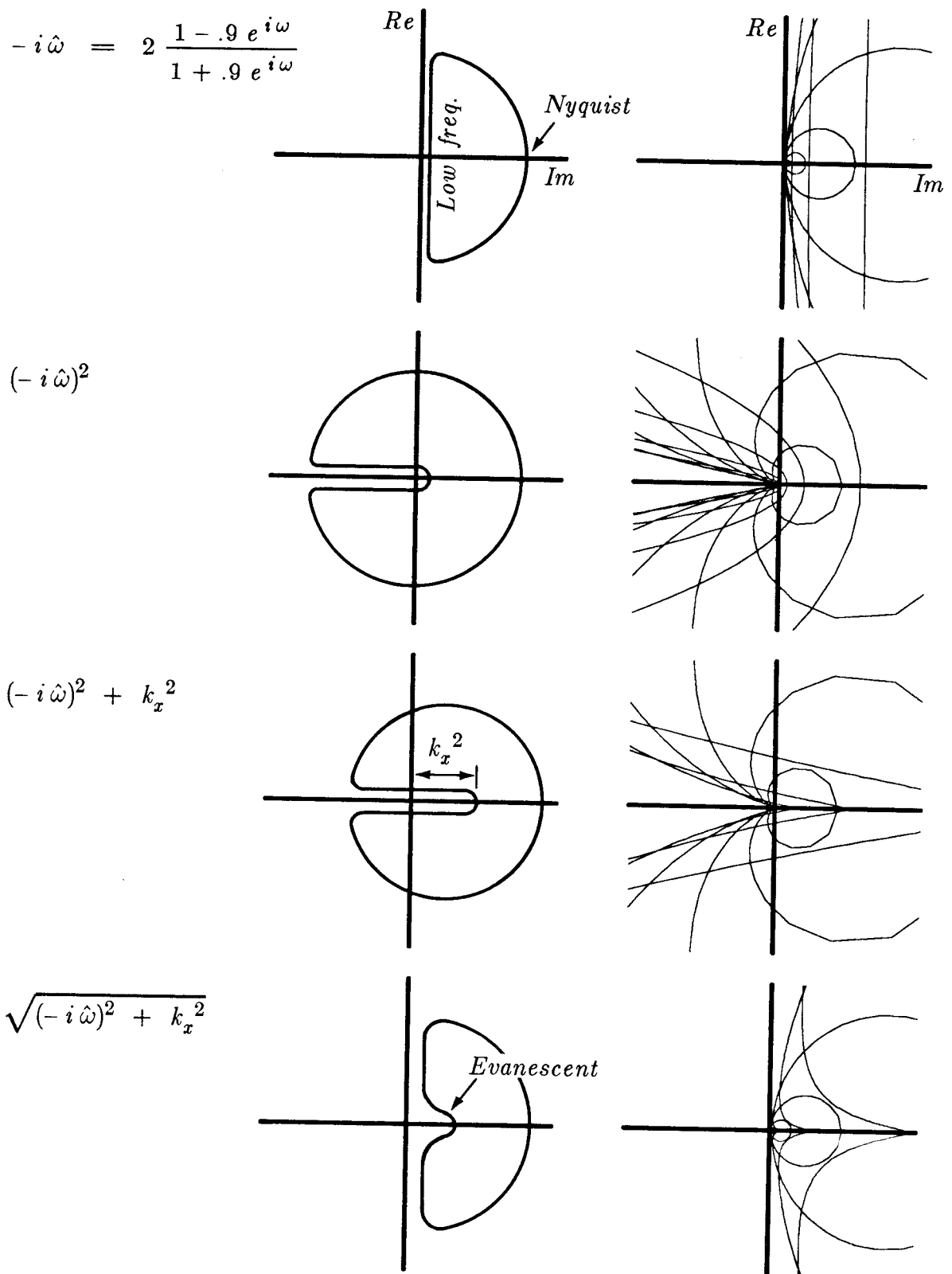


FIG. 4.6-3. Complex plane diagram of constituents of the extrapolation operator  $R$  given by (36). The center column shows an artist's conception. The right column shows the function at several magnifications simultaneously.



### Fractional Integration and Constant $Q$

By equation (29) and theorem 6, fractional powers of integration and differentiation are also impedance functions. Kjartansson [1979] has advocated the fractional power as a stress-strain law for rocks. See also Madden [1976]. Classical studies in rock mechanics begin with a stress-strain law such as

$$\text{stress} = \text{stiffness} \times \text{strain} + \text{viscosity} \times \text{strain-rate}$$

which in the transform domain is

$$\begin{aligned} \text{stress} = [(-i\omega)^0 \times \text{stiffness} + \\ (-i\omega)^1 \times \text{viscosity}] \times \text{strain} \end{aligned} \quad (37)$$

Experimentally, the viscoelastic law (37) does a poor job of describing real rocks. Let us try another mathematical form that is like (37) in its limiting behavior at high and low viscosity:

$$\text{stress} = \text{const} \times (-i\omega)^\epsilon \times \text{strain} \quad (38a)$$

$$= \text{const} \times (-i\omega)^{\epsilon-1} \times \text{strain-rate} \quad (38b)$$

Here  $\epsilon$  close to zero gives elastic behavior and  $\epsilon$  close to one gives viscous behavior. The fact that  $(-i\omega)^{\epsilon-1}$  is an impedance function meshes nicely with the concepts that (1) stress may be determined from strain history and strain may be determined from stress history, and (2) stress times strain-rate is dissipated power. Kjartansson [1979] points out that  $(-i\omega)^\gamma$  exhibits the mathematical property called *constant Q*, so that as a stress/strain law for fitting experimental data on rocks, it is far superior to (37). To see the constant  $Q$  property more clearly, express  $(-i\omega)^\gamma$  in real and imaginary parts:

$$(-i\omega)^\gamma = |\omega|^\gamma [-i \operatorname{sgn}(\omega)]^\gamma \quad (39a)$$

$$= |\omega|^\gamma [e^{-i\pi \operatorname{sgn}(\omega)/2}]^\gamma \quad (39b)$$

$$= |\omega|^\gamma \left\{ \cos \left[ \frac{\pi\gamma}{2} \operatorname{sgn}(\omega) \right] - i \sin \left[ \frac{\pi\gamma}{2} \operatorname{sgn}(\omega) \right] \right\} \quad (39c)$$

$$= |\omega|^\gamma \left[ \cos \left[ \frac{\pi\gamma}{2} \right] - i \operatorname{sgn}(\omega) \sin \left[ \frac{\pi\gamma}{2} \right] \right] \quad (39d)$$

The constant  $Q$  property follows from the constant ratio between the real and imaginary parts of this function.  $Q$  itself is defined by

$$\frac{1}{Q} = \tan \pi\epsilon \approx \pi\epsilon \quad (40)$$

A pulse with a  $Q$  of about 10 is shown in figure 4.

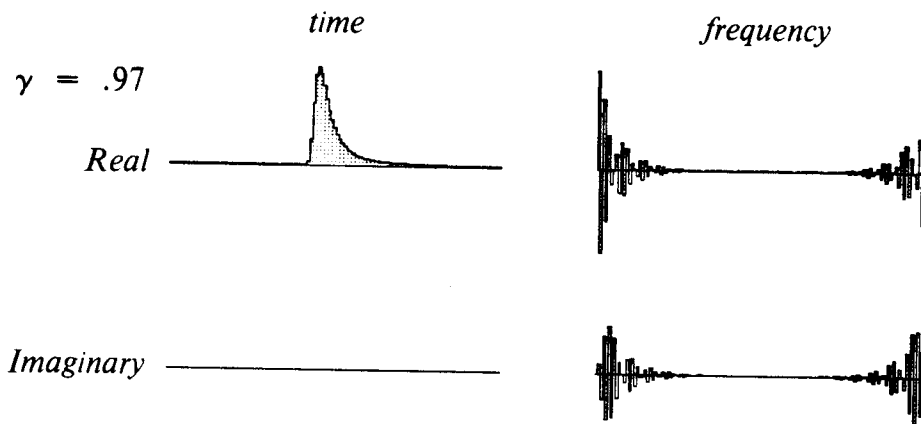


FIG. 4.6-4. The constant  $Q$  pulse given by  $e^{-(-i\omega)^{\gamma}t_0}$ . The frequency axis is represented by a discrete Fourier transform over 256 points. Zero time and zero frequency are on the left end of their respective axes.

### EXERCISES

1. Take  $\epsilon < 0$  and expand the integration operator for negative powers of  $Z$ . Explain the sign difference.
2. Let  $\alpha > 0$  be a real, positive scaling constant, and let  $C$  be a reflectance function. Without using Muir's rules, prove that  $C'$  is a reflectance, where

$$\frac{1 - C'}{1 + C'} = \alpha \frac{1 - C}{1 + C}$$

Note that you have proven Muir's first rule. Muir's third rule can also be proven in an analogous way, but with much more algebraic detail.

3. The word *isomorphism* means not only that any impedance  $R_1, R_2, R'$  can be mapped into a reflectance  $C_1, C_2, C'$ , but also that Muir's three rules will be mapped into three rules for combining reflectances.
  - a. What are these three rules?
  - b. Although  $C' = C_1 C_2$  does not turn out to be one of the three rules, it is obviously true. Either show that it is a consequence of the three rules or conclude that it is an independent rule that can be mapped back into the domain of the impedances to constitute a fourth rule.

4. Show that the log of the discrete causal integration operator,  $\log[(1+Z)/(1-Z)]$ , is one side of the discrete Hilbert transform. Show that the reflected pulse from a boundary between two media with the same velocity but slightly different  $Q$  is one side of the Hilbert transform.
5. Consider the fourth-order Taylor expansion for square root in an extrapolation equation

$$\frac{dP}{dz} = i\omega \left[ 1 - \frac{1}{2} \left( \frac{vk}{\omega} \right)^2 - \frac{1}{8} \left( \frac{vk}{\omega} \right)^4 \right] P$$

- a. Will this equation be stable for the complex frequency  $-i\omega = -i\omega_0 + \epsilon$ ? Why?
  - b. Consider causal and anticausal time-domain calculations with the equation. Which, if any, is stable?
6. Consider a material velocity that may depend on the frequency  $\omega$  and on the horizontal  $x$ -coordinate as well. Suppose that, luckily, the velocity can be expressed in the factored form  $v(x, \omega) = v_1(x) v_2(\omega)$ . Obtain a stable  $45^\circ$  wave-extrapolation equation. Hints: try

$$s = -\frac{i\omega}{v_2}$$

$$X^2 = \text{positive eigenvalue of } (v_1 \partial_x)(v_1 \partial_x)^T$$

7. Is the Levinson Recursion described in FGDP related to the rules in this section? If so, how? Hint: see Jones and Thron [1980].
8. Show the converse to theorem 4, namely, that if the phase curve of a causal function does not enclose the origin, then the inverse is causal.

## 4.7 Accuracy — the Contractor's View

A chain is no stronger than its weakest link. Economy dictates that all the links should be equally strong. Many broad questions merit study such as the errors associated with velocity uncertainty and with migration after, rather than before, stack. Having read this far, you are now qualified to attack these broad questions. Now we will narrow our focus and examine only the errors in downward continuation that result from familiar data processing approximations.

In the construction of a production program for wave-equation migration, weakness arises from approximations made in many different places. Economy dictates that funds to purchase accuracy should be distributed where they will do the most good. Geophysical contractors naturally become experts on accuracy/cost trade-offs in the migration of stacked data. Contractors will use the equations and program gathered below to obtain best results for the lowest cost. Users of reflection data are interested in learning to recognize imperfect migrations, so they may want to use the program to see the effect of various shortcuts.

In preparation for a big production job there are two general approaches to examining accuracy. The first approach, which gives the best insight into qualitative phenomena, is to make synthetic hyperbolas by the various methods. The synthetic hyperboloids can be compared to the data at hand with a video movie system or by plotting on transparent paper. In the second approach you compute travel times of hyperboloids or spheroids of waves of different stepouts and frequencies for different mesh sizes, etc. Then an optimization program can be run to minimize the average error over the important range of parameters.

It is not necessary to write a time domain  $45^\circ$  finite difference migration program to see what its synthetic hyperboloids would look like. We can simply express all the formulas in the  $(\omega, k_x)$ -domain and then do an inverse two-dimensional Fourier transformation. To facilitate comparisons between the many migration methods we will gather equations from different parts of the book in the order that they are needed. Then I'll present the program that makes the diffraction hyperbolas for many methods. Using the same equations you can compute travel times and solve the optimization problem as you wish.

### Lateral Derivatives

First,  $k_x$  will range over  $\pm\pi/\Delta x$ . If the  $x$ -axis is going to be handled by finite differencing then we will need

$$\left( \frac{\hat{k} \Delta x}{2} \right)^2 = \frac{\sin^2 \frac{k \Delta x}{2}}{1 - b \frac{4 \sin^2 \frac{k \Delta x}{2}}{2}} \quad (4.3-7b)$$

So if the  $x$ -axis is going to be handled by finite differencing then subsequent reference to  $k_x$  should be replaced by  $\hat{k}_x$ . The finite differencing introduces the free parameter  $b$ . Likewise, you could also scale the whole expression by an adjustable parameter near unity. Also,  $\Delta x$  isn't necessarily fixed by the data collection. You could always interpolate the data before processing. A finite-difference method using interpolated data could be mandated by enough lateral velocity variation.

### Viscosity and Causality

The frequency  $\omega$  will range over  $\pm\pi/\Delta t$ . If the  $t$ -axis is going to be handled by finite differencing then we will need the  $Z$ -transform variable

$$Z = e^{i \omega \Delta t} \quad (4.6-2)$$

and the causal derivative

$$-i \hat{\omega} = \frac{2}{\Delta t} \frac{1 - \rho Z}{1 + \rho Z} \quad -1 \ll \rho < 1 \quad (4.6-29)$$

The data can be subsampled or supersampled before processing, so  $\Delta t$  is an adjustable parameter. The causality parameter  $\rho$  should be a small amount less than unity, say  $\rho = 1 - \epsilon$  where  $\epsilon > 0$  is an adjustable parameter. You may want to introduce  $\rho$  even if you are migrating in the frequency domain because it reduces wraparound in the time domain — it is a kind of viscosity. The  $\epsilon$  should be about inverse to the data length, say  $1/N_t$  where  $N_t$  is the number of points on the time axis. (Because I made many plots of synthetic hyperbolas with square root gain,  $\gamma = 1/2$ , time wraparounds were larger than life. So I had the program default to  $\epsilon$  four times larger). If you like to adjust free parameters, you could separately adjust numerator and denominator values of  $\rho$ . Subsequently, I'll distinguish between  $\omega$  and  $\hat{\omega}$ , but you can take  $\hat{\omega}$  to be  $\omega$  if you don't care to introduce causality.

### Retarded Muir Recurrence

The  $k_z$  square root may be computed with the square root function in your computer or by Muir's expansion. For Fourier domain calculations incorporating causality, you must use a complex square root function. This will also take care of the evanescent region automatically — you no longer have the discontinuity between evanescent and nonevanescent regions. The square root of a complex number is multivalued, so you better first check that your computer chooses the phase as described in figure 4.6-3. Mine did. But I found that limited numerical accuracy prevented me from achieving strict positivity of the real part of the impedance until I replaced the expression  $\sqrt{s^2 + v^2 k^2} - s$  by its algebraic equivalent  $v^2 k^2 / (\sqrt{s^2 + v^2 k^2} + s)$ .

For finite differencing we will need the Muir recurrence. Let  $r_0$  define the cosine of the angle that starts the Muir recurrence, often  $0^\circ$  or  $45^\circ$ . This is another free parameter for optimization. See for example figure 2.1-1. This angle is also an angle of exact fit for all orders of the recurrence. Let

$$s = -i \hat{\omega} \quad (4.6-29)$$

Starting from  $R_0 = r_0 s$  the Muir recursion is

$$R_{n+1} = s + \frac{v^2 k_x^2}{s + R_n} \quad (4.6-30)$$

For a diffraction program we will be evaluating  $\exp(-Rz)$ . Since  $R$  was proven in 4.6 to have a positive real part, the exponential should never grow. Finite difference calculations are normally done with retarded time. To retard time,  $\exp(-Rz)$  is expressed as

$$e^{-Rz/v} = e^{-(R-s)z/v} e^{-sz/v} \quad (1)$$

As discussed in Section 4.1, you probably don't want the time shift of retardation to be associated with viscous effects. So you will probably want to downward continue instead with

$$e^{-[R(-i\hat{\omega}) + i\hat{\omega}]z/v} = e^{+i\omega z/v} \quad (2)$$

Notice the signs and distinction of  $\omega$  from  $\hat{\omega}$ .

From equation (4.6-30) we see that  $R-s$  should have a positive real part. I found that numerical roundoff sometimes prevented it. So the Muir recurrence was reorganized to incorporate the retardation. Let

$$R' = R - s \quad (3)$$

Equation (4.6-30) becomes

$$R'_{n+1} = \frac{v^2 k_x^2}{2s + R'_n} \quad (4)$$

From Muir's rules, you can see that  $R'$  will always have a positive real part if we start it that way, so we start it from

$$R'_1 = \frac{v^2 k_x^2}{s(1+r_0)} \quad (5)$$

(Combining (5) and (3) gives the same 15° equation as does (4.6-30).) Mathematically (2) is identical to

$$e^{-R'z/v} e^{i\omega z/v} \quad (6)$$

but numerically the exponential in (6) is assured to decay in  $z$ .

### Stepping in Depth

If you are using finite differences on depth, or travel-time depth, then we have the relation

$$\frac{\hat{k}_z \Delta z}{2} = \tan \frac{k_z \Delta z}{2} \quad (4.3-14)$$

which can be used in  $\exp ik_z z$ . Since dissipation may be present, the quantities above may be complex. Let  $N_z$  be the number of depth layers, generally equal or less than  $N_t$ . Adapting (4.3-17) to (6) gives

$$e^{-R' N \Delta z/v} \approx \left( \frac{1 - R' \Delta z/2v}{1 + R' \Delta z/2v} \right)^N \quad (7)$$

### Lightning Phase Shift Migration

Not only can the causality and viscosity features of time domain methods be incorporated in the frequency domain, but the square roots and complex exponentials of the phase shift method can be replaced by complex multiplies and divides. First note that the square root expansion need not begin from a starting guess or from a lower order iteration. It could begin from the square root previously obtained from the preceding  $\omega$  or  $k$ . (I noticed this when an early version of the program had a bug that made all my 15° calculations look like 90° calculations)! Also,  $\Delta z/v$  is necessarily small in the phase shift method to accommodate imaging at every time point. So the finite differencing form (7) is probably as good as the complex exponential. Why

don't you try it?

### Final Appearances

The output of an impulse-response program always looks awful. The main reason is the large area of  $(\omega, k_x)$ -space which is near the Nyquist frequency or above the evanescent cutoff. Since we rarely sample data in time as coarsely as the Nyquist criterion permits, the program below defaults to final filtering with the filter  $(1+Z)/(1-.8Z)$ . This filter still passes a lot of energy outside the usual bandwidth of seismic data. Since all land data and most marine data do not have the zero frequency component, the program contains an option to filter further with  $(1-Z)/(1-.8Z)$ . I haven't displayed anything with this extra filter because I wanted this book to show all the artifacts you might encounter. Furthermore, I deliberately enhanced the visibility of artifacts on wiggle-trace, variable-area plots by plotting with the nonlinear  $\gamma = 1/2$  gain described in Section 4.1. (Perspective hidden-line drawings always have linear gain). Since my plots are necessarily about 10 cm square in this book and in practice you will look at plots of about a hundred times the area, I plotted only one second of travel time.

### Program

Many of the figures in the book were made with the program presented here. To enable you to reproduce them I am including the complete program. The parameter input and data output calls are site dependent, but I include them anyway to help clarify the defaults, increasing the odds that you can get exactly what I did.

```
# representations of  $e^{-\sqrt{(-i\omega/v)^2 + k^2} z}$ 
integer output, outfd, fetch
integer iw,nw,ik,nk, omhat, kxhat, kzhat, degree, tfilt, xfilt
real v, dt, dx, dz, xf, x0, tf, tau0, rho, bi, r0, eps, pi, omega, k, vk2
complex cz, cs, cikz, cexp, cmplx, csqrt, cp(1024)
outfd = output()
nw = 256;      call putch("esize", "i", 8)      # complex numbers
nk = 64;      call putch( "n1", "i", nw)      # inner index is  $\omega$ 
              call putch( "n2", "i", nk)      # outer index is  $k_x$ 
              call putch( "n3", "i", 1)      # one frame movie

if( fetch( "v", "f", v) == 0 ) v = 3.754      # rock vel
if( fetch( "dt", "f", dt) == 0 ) dt = .004    #  $\Delta t$ , sec
if( fetch( "dx", "f", dx) == 0 ) dx = .025    #  $\Delta x$ , km
if( fetch( "dz", "f", dz) == 0 ) dz = .004    #  $\Delta z$ , sec
if( fetch( "xf", "f", xf) == 0 ) xf = .25;    x0 =xf*nk*dx
if( fetch( "tf", "f", tf) == 0 ) tf = .5;    tau0=tf*nw*dt
```



```

if( fetch( "omhat", "i", omhat) == 0 ) omhat = 0      #  $\hat{\omega}$ 
if( fetch( "kxhat", "i", kxhat) == 0 ) kxhat = 0    #  $\hat{k}_x$ 
if( fetch( "kzhat", "i", kzhat) == 0 ) kzhat = 0    #  $\hat{k}_z$ 
if( fetch( "degree", "i", degree) == 0 ) degree = 90
if( fetch( "tflt", "i", tflt) == 0 ) tflt = 1
if( fetch( "xflt", "i", xflt) == 0 ) xflt = 1

if( fetch( "rho", "f", rho) == 0 ) rho = 1-4./nw
if( fetch( "bi", "f", bi) == 0 ) bi = 6.726          #  $b^{-1}$ 
if( fetch( "r0", "f", r0) == 0 ) r0 = 0.7071
if( fetch( "eps", "f", eps) == 0 ) eps = 0.

call putch( "d1", "f", dt);      call putch( "label1", "s", "sec" )
call putch( "d2", "f", dx);      call putch( "label2", "s", "kilometers" )
call hclose()                    # close data description file
pi = 3.14159265
do ik = 1, nk {                  # loop over all  $k_x$ 
    k = 2*pi * (ik-1.) / nk
    if( k > pi ) k = k - 2*pi
    k = k / dx
    if( kxhat == 0 )
        vk2 = (v/2)**2 * k*k
    else
        vk2 = (v/2)**2 * (2/dx)**2 * sin(k*dx/2)**2 / (1 -
            (4./bi) * sin(k*dx/2)**2 )

    do iw = 1, nw {              # loop over all  $\omega$ 
        omega = 2*pi * (iw-1.) / nw
        if( omega > pi ) omega = omega - 2*pi
        omega = omega / dt
        cz = cexp( cmplx( 0., omega * dt ) )
        if( omhat == 0 )
            cs = cmplx( 1.e-5 / dt, - omega )
        else
            cs = (2./dt) * (1. - rho * cz) / (1. + rho * cz)
        if ( degree == 90 )
            cikz = vk2 / ( csqrt( cs * cs + vk2 ) + cs )
        if ( degree == 15 | degree == 45 )
            cikz = vk2 / ( eps + (r0+1.) * cs )
        if ( degree == 45 )
            cikz = vk2 / ( 2.*cs + cikz )
        if( real( cikz ) < 0. ) call erexit( "cikz not positive real" )

        if( kzhat == 0 )
            cp(iw) = cexp( - tau0 * cikz )
        else
            cp(iw) = ((1.-cikz * dz/2) / (1.+cikz * dz/2)) ** (tau0/dz)
            cp(iw) = cp(iw) * cexp( cmplx(0., omega * tau0) ) # unretard

        if( tflt >= 1 ) cp(iw) = cp(iw) * (1+cz) / (1 - .8 * cz)
        if( tflt >= 2 ) cp(iw) = cp(iw) * (1-cz) / (1 - .8 * cz)
        if( xflt == 1 ) cp(iw) = cp(iw) * (1+cos(k*dx)) / (1+.85*cos(k*dx))
        cp(iw) = cp(iw) * cexp( cmplx(0.,k*x0) )
    }
    call rite( outfd, cp, 8*nw ) # write
}
}
stop; end
# Finally, you must 2-D Fourier Transform (Section 1.7), take real part, and plot.

```

Twenty-two plots displayed in this book were made with this program. Different input parameters for the different plots are in the table below.

Section and figure.	Default parameter overrides.
1.3-6a	tfilt=0
1.3-6b	
2.0-1a	
2.0-1b	$\hat{\omega}$
4.0-1a	$\hat{\omega}, v = 2.0, \text{xf}=.5, \text{xfilt}=0$
4.0-1b	$\hat{\omega}, v = 2.0, \text{xf}=.5$
4.1-4a	$15^\circ$
4.1-4b	$15^\circ, \epsilon = 1$
4.1-5a	$45^\circ, \text{tf}=.2$
4.1-5b	$45^\circ, \text{tf}=.2, \epsilon = 1$
4.2-4	$45^\circ, \text{tf}=.2, \hat{\omega}$
4.3-4a	$v = 2.0, 90^\circ$
4.3-4b	$v = 2.0, 15^\circ, \hat{\omega}, \hat{k}_x, \hat{k}_z$
4.3-6a	$\hat{k}_x, \hat{\omega}, b^{-1}=1000000.$
4.3-6b	$\hat{k}_x, \hat{\omega}, b^{-1}=12.$
4.3-6c	$\hat{k}_x, \hat{\omega}, b^{-1}=6.726$
4.3-6d	$\hat{k}_x, \hat{\omega}, b^{-1}=6.$
4.3-6e	$\hat{k}_x, \hat{\omega}, b^{-1}=5.$
4.6-2a	
4.6-2b	$\hat{\omega}$
4.7-1a	$\Delta z = .004, 45^\circ, \text{tf}=.3, \hat{\omega}, \hat{k}_x, \hat{k}_z$
4.7-1b	$\Delta z = .012, 45^\circ, \text{tf}=.3, \hat{\omega}, \hat{k}_x, \hat{k}_z$

It is rumored that accuracy can be improved by making the  $z$  mesh coarser. This couldn't happen if  $x$  and  $t$  were in the continuum, but since they may be discretized, there is the possibility of errors fortuitously canceling. To test this rumor, I tried tripling  $\Delta z$  (actually, tripling the increment in travel-time depth). The result is in figure 1. What do you think?

Complete as this analysis must seem, it is limited by the assumption of Fourier analysis that velocity is constant laterally. To handle this problem we turn now to the final lecture on techniques.

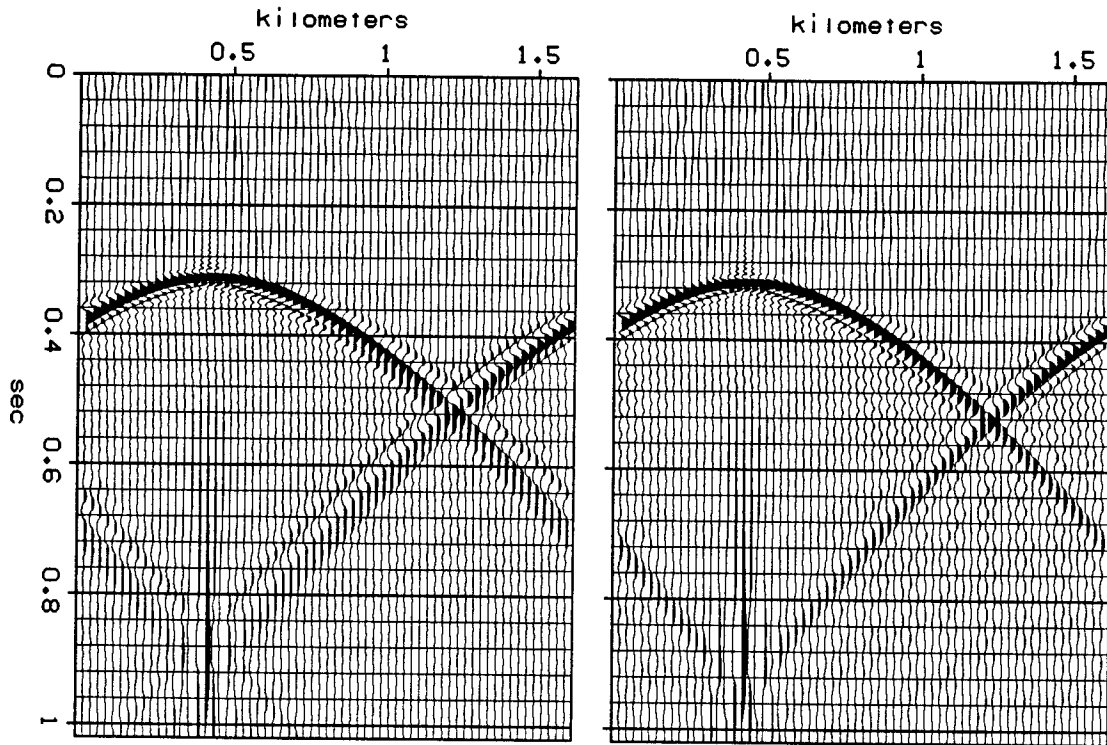


FIG. 4.7-1. Left is a  $45^\circ$  point diffraction in  $(x, z, t)$ -space with  $\Delta z = v \Delta t$ . At the right, with  $\Delta z = 3v \Delta t$ .

## 4.8 The Bulletproofing of Muir and Godfrey

Stable extrapolation can be assured by preserving certain symmetries. It will be shown that stability is assured in both the differential equation

$$\frac{d\mathbf{q}}{dz} = -\mathbf{R}\mathbf{q} \quad (1)$$

and its Crank-Nicolson approximation

$$\frac{\mathbf{q}_{n+1} - \mathbf{q}_n}{\Delta z} = -\frac{\mathbf{R}}{2}(\mathbf{q}_{n+1} + \mathbf{q}_n) \quad (2)$$

provided that  $\mathbf{R} + \mathbf{R}^*$  is a positive definite (actually, semidefinite) matrix. When stability was studied in the previous section the operator  $\mathbf{R}$  was a scalar  $Z$ -transform. Because  $Z$ -transforms were used, the mathematics of that section was particularly suitable for time domain migrations. Because  $\mathbf{R}$  was a scalar, the mathematics of that section was particularly suitable when

data has been Fourier transformed over  $x$ . Here we will focus on the *matrix* character of  $\mathbf{R}$ . Thus we are concerning ourselves with migration in the  $x$ -domain. Our purpose in doing this theoretical work is to gain the ability to write a "bulletproof" program for migrating seismic data in the presence of lateral velocity variation. As an example, the familiar  $45^\circ$  extrapolation equation will be put in the bulletproof form. This section, combined with the previous one, gives a general theory for stable migration in  $(t, x)$ -space.

### Stability of the Differential Equation

Let  $\mathbf{q}^*$  denote the Hermitian conjugate of  $\mathbf{q}$ . For equation (1) to be stable the energy  $\mathbf{q}^* \mathbf{q}$  must be either constant or decaying during depth extrapolation.

$$\begin{aligned} \frac{d}{dz} (\mathbf{q}^* \mathbf{q}) &\leq 0 \\ \mathbf{q}^* \mathbf{q}_z + \mathbf{q}_z^* \mathbf{q} &\leq 0 \end{aligned} \quad (3)$$

Substituting equation (1) into equation (3) gives

$$\begin{aligned} \mathbf{q}^* \mathbf{R} \mathbf{q} + \mathbf{q}^* \mathbf{R}^* \mathbf{q} &\geq 0 \\ \mathbf{q}^* (\mathbf{R} + \mathbf{R}^*) \mathbf{q} &\geq 0 \end{aligned} \quad (4)$$

Equation (4) shows that  $\mathbf{R} + \mathbf{R}^*$  must be positive semidefinite for the differential equation to be stable.

### Stability of the Difference Equation

The stability of the difference equation can be shown in a similar way, but with some extra clutter. First observe the identity

$$(\mathbf{a}^* \mathbf{a} - \mathbf{b}^* \mathbf{b}) \equiv \frac{1}{2} [(\mathbf{a} + \mathbf{b})^* (\mathbf{a} - \mathbf{b}) + (\mathbf{a} - \mathbf{b})^* (\mathbf{a} + \mathbf{b})] \quad (5)$$

Letting  $\mathbf{a} = \mathbf{q}_{n+1}$  and  $\mathbf{b} = \mathbf{q}_n$ , equation (5) becomes

$$\begin{aligned} (\mathbf{q}_{n+1}^* \mathbf{q}_{n+1} - \mathbf{q}_n^* \mathbf{q}_n) &= \\ &= \frac{1}{2} [(\mathbf{q}_{n+1} + \mathbf{q}_n)^* (\mathbf{q}_{n+1} - \mathbf{q}_n) + (\mathbf{q}_{n+1} - \mathbf{q}_n)^* (\mathbf{q}_{n+1} + \mathbf{q}_n)] \end{aligned} \quad (6)$$

Now, replace the  $(\mathbf{q}_{n+1} - \mathbf{q}_n)$  terms by equation (2):

$$\begin{aligned} &= -\frac{\Delta z}{4} [(\mathbf{q}_{n+1} + \mathbf{q}_n)^* \mathbf{R} (\mathbf{q}_{n+1} + \mathbf{q}_n) + \\ &\quad (\mathbf{q}_{n+1} + \mathbf{q}_n)^* \mathbf{R}^* (\mathbf{q}_{n+1} + \mathbf{q}_n)] \end{aligned}$$

$$= -\frac{\Delta z}{4} [(\mathbf{q}_{n+1} + \mathbf{q}_n)^* (\mathbf{R} + \mathbf{R}^*) (\mathbf{q}_{n+1} + \mathbf{q}_n)] \quad (7)$$

This equation establishes the result: If the matrix  $\mathbf{R} + \mathbf{R}^*$  is positive definite, then  $\mathbf{q}_{n+1}^* \mathbf{q}_{n+1}$  is less than  $\mathbf{q}_n^* \mathbf{q}_n$ .

### Application to 45° Wavefield Extrapolation

The scalar wave equation for the extrapolation of a downgoing wavefield is

$$\frac{d\mathbf{q}}{dz} = i k_z \mathbf{q} = -\mathbf{R} \mathbf{q} \quad (8)$$

where the  $\mathbf{R}$  operator takes the usual form

$$\mathbf{R} = -i k_z = \frac{-i\omega}{v} \sqrt{1 - \frac{v^2 k_x^2}{\omega^2}} \quad (9)$$

Our plan is to approximate the square root by the usual continued fraction expansion and then identify  $i k_z$  with  $\partial_x$  to obtain a space-domain equation. The main effort we must make stems from our refusal to make the usual assumption that  $v(x, z)$  is independent of  $x$ . Since  $\partial_x v q$  differs from  $v \partial_x q$ , the space representation does not seem to be unique, and we may wonder how the variable  $q$  relates to physical wave variables like pressure and displacement. Since (9) is purely imaginary, the depth-invariance of the quadratic  $\mathbf{q}^* \mathbf{q}$  can be interpreted as the downward energy flux across the datum at depth  $z$ . Our main effort will be to assure that  $\mathbf{q}^* \mathbf{q}$  does indeed remain depth-invariant when  $v(x, z) \neq \text{const}$ . The task of determining the relation between the energy flux variable  $\mathbf{q}$  and the physical variables will be left to the reader.

First  $v^2 k_x^2$  must be represented in the space domain. Thinking of the  $x$ -derivative operator  $\partial/\partial x = \partial_x$  as a large bidiagonal matrix with  $(1, -1)/\Delta x$  along the diagonal and  $\mathbf{V}(x)$  as a diagonal matrix, we are attracted to expressions like  $(\mathbf{V} \partial_x)^T (\mathbf{V} \partial_x)$  or  $(\mathbf{V} \partial_x) (\mathbf{V} \partial_x)^T$  because they are symmetric, positive, semidefinite matrices. In simplest form, such numerical representations are tridiagonal matrices that can be abbreviated as

$$\mathbf{T} = \begin{cases} (\mathbf{V} \partial_x) (\mathbf{V} \partial_x)^T \\ (\mathbf{V} \partial_x)^T (\mathbf{V} \partial_x) \end{cases} \quad (10a,b)$$

At a later time accuracy or some other consideration could determine the

choice in (10). Even other expressions could be used, provided they are real, symmetric, and positive definite.

In the previous section the constant velocity, 45° expansion of (9) was shown to be

$$\mathbf{R} = \frac{1}{v} \frac{v^2 k_x^2}{-i\omega 2 + \frac{v^2 k_x^2}{-i\omega 2}} \quad (11)$$

This scalar  $\mathbf{R}$  always has a positive real part because  $-i\omega$  is always represented in an impedance form, and the whole expression is built up satisfying Muir's rules for combining impedance functions. In going to the  $x$ -domain notice that  $(i k_x)^2 = -\partial_{xx}$  and  $(\partial_x)^T = -\partial_x$ . So the positive scalar  $v^2 k_x^2$  corresponds to the positive eigenvalues of (10).

The expression of the bulletproof, square-root operator  $\mathbf{R}$  in the space domain will now be given as

$$\mathbf{M} = \frac{\mathbf{T}}{-i\omega 2 \mathbf{I} + \frac{\mathbf{T}}{-i\omega 2}} \quad (12a)$$

$$\mathbf{R} = \mathbf{V}^{-1/2} \mathbf{M} \mathbf{V}^{-1/2} \quad (12b)$$

Use of the division sign in (12) is justifiable because the matrix  $\mathbf{T}$  commutes with the identity matrix  $\mathbf{I}$ . (A hazard in this work is that  $\mathbf{T}$  does not commute with the diagonal matrix  $\mathbf{V}$ ). The matrix  $\mathbf{M}$  has the properties required of  $\mathbf{R}$  since a basic matrix theorem says that the eigenvalues of a polynomial of a real symmetric matrix are the polynomials of the eigenvalues. In other words, replacing  $\mathbf{T}$  in (12) by one of its eigenvalues produces a complex  $\mathbf{M}$  whose real part is positive, so that  $\mathbf{M}^* + \mathbf{M}$  is positive as required. What is needed is to show that the following matrix is positive definite:

$$\mathbf{R} + \mathbf{R}^* = \mathbf{V}^{-1/2} (\mathbf{M} + \mathbf{M}^*) \mathbf{V}^{-1/2} \quad (13)$$

A matrix  $\mathbf{A}$  is positive definite if for arbitrary  $d$ , the scalar  $d^* \mathbf{A} d$  is positive. The diagonal matrix  $\mathbf{V}^{-1/2}$  can certainly be absorbed into  $d$  and  $d$  will still be arbitrary, so the proof is complete.

In programming it is a nuisance to put  $\mathbf{V}^{-1/2}$  on each side of the matrix  $\mathbf{M}$ . Actually you can put  $\mathbf{V}^{-1}$  on either side. In general, some other quadratic form such as  $\mathbf{q}^* \mathbf{U} \mathbf{q}$  where  $\mathbf{U}$  is strictly positive definite will be decreasing if  $\mathbf{R}^* \mathbf{U} + \mathbf{U} \mathbf{R}$  is positive definite.